Title: $CD8^+$ T-cell memory induced by successive SARS-CoV-2 mRNA vaccinations is characterized by clonal replacement

Authors: Hiroyasu Aoki[1,2], Masahiro Kitabatake[3], Haruka Abe[1], Peng Xu[1], Mikiya Tsunoda[1], Shigeyuki Shichino[1], Atsushi Hara[3], Noriko Ouji-Sageshima[3], Chihiro Motozono[4], Toshihiro Ito[3], Kouji Matsushima[1], and Satoshi Ueha[1]*

Affiliations:

[1] Division of Molecular Regulation of Inflammatory and Immune Diseases, Research Institute for Biomedical Sciences, Tokyo University of Science, Chiba, Japan.

[2] Department of Preventive Medicine, Graduate School of Medicine, The University of Tokyo.

[3] Department of Immunology, Nara Medical University, Nara, Japan.

[4] Division of Infection and Immunity, Joint Research Center for Human Retrovirus Infection, Kumamoto University, Kumamoto, Japan.

*Satoshi Ueha, Ph.D., Division of Molecular Regulation of Inflammatory and Immune Diseases, Research Institute for Biomedical Sciences, Tokyo University of Science,

2669 Yamazaki, Noda City Chiba, 278-0022, Japan

E-mail; ueha@rs.tus.ac.jp

Abstract

mRNA vaccines against the Spike glycoprotein of severe acute respiratory syndrome type 2 coronavirus (SARS-CoV-2) elicit strong T-cell responses. However, it's not known whether T cell clonotypes responding to the first vaccination repeatedly expand with booster vaccinations. Here, we temporally tracked the $CD8^+$ T-cell repertoire in individuals who received three shots of the BNT162b2 mRNA vaccine. By analyzing the kinetic profile of $CD8^+$ T-cell clonotypes responding to the first, second, or third shot, we demonstrated that newly expanded clonotypes elicited by the second shot replaced many of those that responded to the first shot. Although these 2nd responder clonotypes expanded after the third shot, their clonal diversity was skewed, and they were partially replaced by newly elicited the 3rd responders. Furthermore, this replacement of vaccine-responding clonotypes occurred within the same Spike epitope. These results suggest that $CD8^+$ T-cell memory induced by repetitive mRNA vaccination is characterized by the emergence of new dominant clones.

Introduction

mRNA vaccines against the Spike glycoprotein of severe acute respiratory syndrome type 2 coronavirus (SARS-CoV-2), including Pfizer-BioNTech's BNT162b2 and Moderna's mRNA-1273, are strikingly effective at reducing coronavirus disease 2019 (COVID-19)[1]. These mRNA vaccines elicit both humoral and cellular immune responses specific for the viral Spike protein[2–4]. The cellular immune response may be more protective to variants of concerns (VOCs) of SARS-CoV-2 than the humoral response, because cellular immunity against the ancestral strain targets relatively conserved regions of the Spike protein[5,6] and potentially cross-reacts with the other variants[7,8]. Studies on the cellular immune responses to SARS-CoV-2 mRNA vaccination have demonstrated that the numbers of Spike-reactive T cells increase in the peripheral blood after the first shot, and are additionally boosted after the second shot[4,9,10]. Furthermore, the third mRNA vaccination rapidly re-expands Spike-reactive T cells that had waned after the second shot[11,12].

Previous studies demonstrated that secondary, or boost, vaccinations induce the reactivation of memory $CD8^+$ T cells established following the initial vaccination[13–16]. However, repetitive antigen stimulation in mice alters the properties of memory T cells, including enhancement of their effector function, and reductions in their proliferation

55 potential and ability to produce IL-2[14,17]. This suggests that memory $CD8^+$ T cells
56 induced by the first vaccination become poorly, or non-responsive during the course of
57 repetitive antigen stimulation. In line with this hypothesis, we previously reported that
58 older memory T cell populations were replaced by newly expanded T cell populations in
59 a serial adoptive transfer model characterized by repetitive antigen exposure[18].
60 However, in repetitive SARS-CoV-2 mRNA vaccinations, it is not known whether T
61 cell clonotypes that had responded to the first shot expanded repeatedly after subsequent
62 vaccination, or whether primary responder clonotypes were partially, or fully, replaced
63 by newly expanded clonotypes after each vaccination.
64 Pathogen-reactive T cells recognize distinct antigenic epitopes via their unique T cell
65 receptor (TCR). To analyze changes in T cell clonal dominance during SARS-CoV-2
66 mRNA vaccination, we undertook a longitudinal repertoire analysis by TCR
67 sequencing. This enabled us to comprehensively quantify changes in the frequencies of
68 specific T-cell clones ("kinetic profile") during primary and secondary responses to
69 mRNA vaccination. Specifically, we performed a longitudinal TCR repertoire analysis
70 on peripheral blood T cells at ten time points, before and after the first, second, and third
71 BNT162b2 mRNA vaccination. Furthermore, Spike reactivity, immunological
72 phenotype, and epitope specificity of T cell clonotypes were analyzed by an activation-

73 induced marker assay (AIM assay) using a Spike peptide pool, single-cell analysis of

74 gene expression and TCR sequence, and TCR motif analysis of Spike-specific T-cell

75 clonotypes.

76

77 **Results**

78 **Novel clones dominated the T-cell response after the second vaccination.**

79 We studied a cohort of 38 healthcare workers at Nara Medical University (Japan) who

80 had received three shots of the Pfizer-BNT162b2 vaccine[19] (Supplementary Table S1).

81 Peripheral blood mononuclear cell (PBMC) samples were longitudinally collected from

82 the participants at ten points (Fig. 1A). $CD4^+$ and $CD8^+$ T cells were separated from the

83 PBMC samples, and their TCR repertoire was analyzed ("bulk TCR repertoire

84 analysis"). To analyze the kinetics of T cell clonal responses to mRNA vaccination, we

85 first compared the frequency of clonotypes before and after the vaccination (P1-P2, P2-

86 P3, and P6-P8). We then identified clonotypes that significantly expanded after each

87 vaccination (i.e., vaccine-responding clonotype) (Figure 1B)[20]. For both $CD4^+$ and

88 $CD8^+$ T cells, the total frequency and diversity of clonotypes that expanded after the

89 second shot was greater than that of responding clonotypes to the first and third shots

90 (Figure 1C and D). This result demonstrated that the T cell clonal response to mRNA

91 vaccination peaked after the second shot.

92 Using the longitudinal bulk TCR-seq data, we analyzed which of the following two
93 models explained the T-cell responses following mRNA vaccinations: (i) repetitive
94 expansion model, in which the clonotypes responded to the first shot expanded
95 repeatedly after the second and third shot, or (ii) clonal replacement model, in which
96 primary responder clonotypes were partially or fully replaced by newly expanded ones
97 after each shot (Figure 1E). For this purpose, the responding clonotypes were classified
98 into four patterns based on their response to each shot (Figure 1F and Figure S1A): 1st
99 responders (expanded after the first shot but did not after the second shot), 2nd
100 responders (did not expand after the first shot but expanded after the second shot), dual
101 responders (expanded or increased after both the first and the second shot), and 3rd
102 responders (were not detected before the third shot and responded to the third shot)
103 (Materials and Methods). Then, the clonal response of each subject was summarized by
104 calculating the total frequency of the clonotypes in each response pattern (Figure 1F,
105 bold line). We longitudinally tracked the total frequency of each response pattern
106 (Figure 1G). After the first shot, the total frequency of the 1st and dual responders was
107 significantly higher than that of the 2nd responders. On the other hand, after the second
108 shot, the total frequency of 2nd responders exceeded the 1st and dual responders (Figure

109 1H). The fact that the 2nd responders, not the dual responders, were dominant after the
110 second shot suggests that, after the second shot, the majority of the responding
111 clonotypes were new clonotypes. The total frequency of responders after the third shot
112 was also analyzed (Figure 1H). At this point, although the expansion of 3rd responders
113 was observed, the 2nd responders were still dominant, and their total frequency was
114 more than twenty times that of 3rd responders. This result demonstrated that most of the
115 responding clonotypes were maintained between the second and third shots, unlike the
116 predominant replacement observed between the first and second shots. A similar
117 replacement of responding clones was also observed in $CD4^+$ T cells (Figure S1A and
118 B).
119

120 **2nd responders were more dominant in $CD8^+$ Spike-reactive clonotypes than dual**
121 **responders**

122 Next, we analyzed whether the predominant replacement of responding clonotypes
123 between the first and the second vaccination was also observed among Spike-reactive
124 clones (Figure 2A). To detect Spike-reactive clonotypes, an activation-induced marker
125 (AIM) assay was performed[9,21–23]. PBMCs collected after the vaccinations (P2, P3, and
126 P8) were stimulated with peptide pools of the SARS-CoV-2 Spike protein. Then,

127 CD137$^+$ or CD107a$^+$ non-naïve CD8$^+$ T cells and CD40L$^+$ CD69$^+$ non-naive CD4$^+$ T

128 cells were sorted as AIM$^+$ Spike-reactive cells (Figure 2B and Figure S2A). The

129 proportion of AIM$^+$ cells among CD8$^+$ and CD4$^+$ T cells quantified by flow cytometry

130 peaked after the second shot, consistent with the numbers and extent of expansion of

131 responding clonotypes in the CD8$^+$ and CD4$^+$ T-cell repertoire (Figure S2B, Figure 1C,

132 and 1D). We then performed TCR-seq on AIM$^+$ and AIM$^-$ non-naive T cells from the

133 samples after the second shot (P3) and identified AIM$^+$ CD8$^+$ and CD4$^+$ T cell

134 clonotypes ("AIM TCR-seq," Figure 1A, 2C, and D). The total frequency of AIM$^+$

135 clonotypes was significantly increased, not only after the second shot, but also after the

136 third shot (Figure 2E and Figure S2C). This observation confirms that CD8$^+$ and CD4$^+$

137 AIM$^+$ clonotypes include Spike-reactive clonotypes responded to the vaccination.

138 We next classified AIM$^+$ clonotypes into the response patterns described above (Figure

139 2F). In addition, we calculated the proportions of 1st, 2nd, and dual responders among

140 CD8$^+$ AIM$^+$ clonotypes (i.e., the number of AIM$^+$ 1st, 2nd, or dual responder clonotypes

141 divided by the total number of AIM$^+$ clonotypes). More than half of the CD8$^+$ AIM$^+$

142 clonotypes were not classified as responders, suggesting that some non-Spike-reactive

143 bystander clonotypes contaminated the AIM$^+$ clonotypes. At the same time, the

144 proportion of the CD8$^+$ 2nd responders was significantly higher than that of AIM$^+$ dual

145 responders (Figure 2G). Moreover, the total frequency of AIM$^+$ 2nd responders of CD8$^+$
146 T cells was also considerably greater than that of AIM$^+$ dual responders after the second
147 shot (Figure 2H). These results indicate that the predominant replacement of responding
148 clonotypes between the first and the second shot also occurred among Spike-reactive T
149 cells. Similar results were observed for CD4$^+$ AIM$^+$ T cell clonotypes (Figure S2D and
150 E).
151
152 **2nd responder clonotypes exhibit effector memory phenotype after the second and**
153 **third vaccination**
154 Our data demonstrate that 2nd responder clonotypes predominate in T cell responses
155 after the second and the third vaccination. Therefore, we next analyzed the phenotype of
156 2nd responders after the second and the third vaccination. Targeted single-cell RNA-
157 sequencing (scRNA-seq), single-cell TCR sequencing (scTCR-seq), and protein
158 expression analysis using oligo-conjugated antibodies (AbSeq) were performed on
159 blood CD8$^+$ T cells of seven participants collected after the second or third vaccination
160 (P3 and P8) (Figure 3A, S3A, and Supplementary Table S2). After removing γδ T cells
161 and mucosal-associated invariant T cells (MAITs), we categorized conventional non-
162 naïve CD8$^+$ T cells into six clusters using integrated mRNA and surface protein

163 expression data (Figure 3B and Figure S3A). We then evaluated the characteristics of
164 these clusters based on the mRNA and protein expression levels of marker genes
165 (Figure 3C, 3D, S3B, and S3C) and signature scores for previously reported blood $CD8^+$
166 T cell clusters[24] and $CD8^+$ T cell characteristics (BD Immune response panel, Hs)
167 (Figure S3D and S3E). Cluster 3 cells expressed *TCF7*, CCR7, and CD127, and
168 exhibited a higher score for stem-like and progenitor-exhausted T cells, which were
169 considered to be central memory T cells (T_{CM}). In addition, we regarded Cluster 2 cells
170 as effector-memory T cells (T_{EM}), because they expressed *CCR5*, *CD38*, and HLA-DR,
171 and exhibited a higher score for EM-like T cells. Moreover, this cluster included
172 *TOP2A*$^+$ proliferating T cells. Cells in the remaining four clusters (#0, 1, 4, and 5) were
173 $CD45RA^{high}$, *GZMB*^{high}, and $CCR7^{low}$, and exhibited higher effector function scores,
174 matching the characteristics of effector memory T cells expressing CD45RA
175 (T_{EMRA})[25,26]. Among them, cluster 0 cells were terminal effector (T_{TE}), based on their
176 expression of CD56 and *GNLY*, and clusters 4 and 5 cells were named OX40 $(CD134)^+$
177 and $Tim3^+$ by their surface marker expression, respectively. Finally, we named cluster 1
178 cells transitory (Trans.) T cells because this cluster exhibited an intermediate phenotype
179 between T_{EM} and T_{TE} clusters. The clonality of these $CD8^+$ T-cell clusters was
180 calculated from the size distribution of clonotypes determined by scTCRseq. These data

181 indicated that clusters 0 and 1 were primarily comprised of oligoclonal T cells, while
182 cluster 3 was primarily comprised of polyclonal T cells (Figure S3F). This tendency in
183 clonality was consistent after the second and third vaccinations.
184 To analyze the phenotype of 2nd responder clonotypes, the 1st, 2nd, and dual responder T
185 cells were plotted in a dimensionality reduction plot (Figure 3E). This analysis revealed
186 that over 90% of T cells in 2nd responder clones exhibited a T_{EM} phenotype after the
187 second shot. On the other hand, the proportion of T_{EM} cells was lower in 1st and dual
188 responders (30. 8% and 76.6 %, respectively) (Figure 3F). Furthermore, the proportion
189 of T_{EM} in the 2nd responders was nearly unchanged after the third shot (94.2% after the
190 second shot, and 92.7 % after the third shot) (Figure 3F). These results demonstrate that
191 2nd responders are mainly comprised of T_{EM} cells after the second and third vaccination.
192 We also identified differentially expressed genes in 2nd responder T_{EM} cells between the
193 second and third shots to examine their shift of gene expression profile (Figure 3G).
194 Genes whose expression was significantly decreased after the third shot included genes
195 associated with the cell cycle (*TYMS* and *MCM4*), transcription factors associated with
196 memory formation (*BACH2* and *STAT3*)[27,28], and costimulatory receptors (*CD28*, *ICOS*,
197 and *DPP4* (coding CD24))[29,30]. Moreover, T_{EM} cells in the 2nd responder pool exhibited
198 higher scores for the TE-like T cells and effector function after the third shot (Figure

199 3H). These results suggest that, although still exhibiting T_{EM} phenotype, 2nd responders

200 are more differentiated towards a T_{EMRA}-like phenotype after the third shot.

201

202 **Skewed re-expansion of 2nd responder clonotypes after the third shot**

203 Next, we analyzed the changes in the repertoire of 2nd responders after the second and

204 the third shot in more detail. The total frequency and fold expansion of 2nd responders

205 after the third shot was significantly decreased compared to that after the second shot

206 (Figure 4A and S4A), suggesting that the expansion of 2nd responders was diminished

207 after the third shot. Notably, the count of expanded clonotypes after the third shot within

208 2nd responders ("re-expanded 2nd responders") was significantly lower than the total

209 count of 2nd responders (Figure 4B): the proportion of re-expanded 2nd responders was

210 only about 30% (Figure S4B). These re-expanded 2nd responder clonotypes were present

211 at a higher frequency after the second shot than 2nd responders that did not expand

212 ("Unchanged") or were not detected after the third shot (Figure S4C). In line with the

213 reduction of expanding clonotypes among 2nd responders, the relative distribution of 2nd

214 responder clonotypes was also changed after the third shot: their clonality was increased

215 while the evenness of their distribution was decreased (Figure 4D). On the other hand,

216 the appearance of the 3rd responders (about 5% of 2nd responder clonotypes, Figure

217 S4B), partially rescued the decreased diversity of the 2nd responders. These changes in

218 CD8+ 2nd responders were also observed in CD4+ T cell repertoire (Figure S4D-H).

219 Based on these results, we modeled the response of CD8+ T-cell clonotypes to mRNA

220 vaccination (Figure 4E). After the second shot, novel responding clonotypes (2nd

221 responders) largely replaced the clonotypes that expanded after the first shot (1st

222 responders) and dominated the responses. After the third shot, a subset of 2nd responders

223 expanded again resulting in a narrowing of the repertoire (i.e. a reduction in the number

224 of re-expanded clonotypes). At the same time, 3rd responders appeared after the third

225 shot and partially compensated for the decrease in 2nd responders' diversity.

226

227 **Induction of CD8+ 2nd responders was associated with anti-RBD antibody titers**

228 **induced by the vaccination.**

229 Next, we analyzed the association between the T cell repertoire and other variables,

230 including the participants' background, anti-SARS-CoV-2 Spike receptor-binding

231 domain (RBD) IgG antibody titer, and strength of the adverse events (Figure 5A).

232 Before doing so, we identified mutually correlated repertoire parameters (e.g., the total

233 frequency of CD8+ dual responder at P2, P3, and P8) and merged them into repertoire

234 meta-parameters (e.g., CD8+ Dual Responders: DualResp) (Figure 5B and S5A,

235 Materials and Methods). The correlation heatmap between $CD8^+$ repertoire meta-
236 parameters and variables related to vaccine response revealed that the total frequency of
237 2nd responders after the second and the third shot ("2^{nd}Resp_P3" and "2^{nd}Resp_P8")
238 was positively correlated with the anti-RBD antibody titers after the second and the
239 third shot, respectively (Figure 5C). Notably, 2^{nd}Resp_P3 was significantly correlated
240 with the antibody titer to RBD of the Omicron variant (Figure 5D). These results imply
241 that some participants respond more readily to mRNA vaccination. At the same time,
242 the total frequency of 1st responders ("1^{st}Resp") was positively associated with the
243 severity of adverse events after the vaccination (Figure 5C). As for $CD4^+$ T cells, the
244 positive correlation between the repertoire meta-parameters and the severity of adverse
245 events was also shown (Figure S5B). These observations are consistent with the study
246 reporting the association between the T-cell response and the severity of adverse
247 reactions following mRNA-1273 vaccination[31]. Finally, we observed a positive
248 correlation between the related meta-parameters between $CD8^+$ and $CD4^+$ T-cell
249 repertoire; $CD8^+$ 3^{rd}Resp and $CD4^+$ 3^{rd}Resp, $CD8^+$ ExpDiv_P8 and $CD4^+$ 2^{nd}Resp_P8,
250 $CD8^+$ AIM and $CD4^+$ AIM or 2^{nd}Resp_AIM, and so on (Figure S5C). This result
251 implies that the clonal responses of $CD4^+$ and $CD8^+$ T cells to the mRNA vaccine are
252 partly coordinated. Notably, we observed no significant association between $CD4^+$ and

253 $CD8^+$ repertoire meta-parameters and sex, history of SARS-CoV-2 infection, or the

254 presence of specific HLA genotypes.

255

256 **Temporal kinetics of T-cell clonotypes were analyzed within Spike epitopes**

257 The results above demonstrate that the replacement of vaccine-responding clonotypes

258 occurred between the first and the second shot. However, it remained unknown how this

259 clonal replacement occurred (Figure 6A). One working hypothesis is "inter-epitope

260 replacement," in which different epitopes induce the 1st and 2nd responder clonotypes.

261 The other hypothesis is "intra-epitope replacement," in which both 1st and 2nd responder

262 clonotypes exist in T cells specific to the same Spike epitope. To determine whether

263 these two models explained the observed clonal replacement, we analyzed the temporal

264 kinetics of Spike-specific T-cell clonotypes at an individual epitope level.

265 For this purpose, two SARS-CoV-2 Spike epitopes were selected (S_{448} and S_{1208}). These

266 two epitopes are reported as immunodominant[32–34] and presented by HLA-A24:02, the

267 most frequent HLA class I allele in an Asian population. Then we prepared peptide-

268 MHC (pMHC) tetramers and identified S_{448}- or S_{1208}-specific $CD8^+$ T cells from

269 $A24{:}02^+$ participants using flow cytometry (Figure 6B and S6A). The positivity of S_{448}-

270 specific cells among $CD8^+$ T cells increased after the first shot, while that of S_{1208}-

271 specific cells increased only after the second shot (Figure S6B). Moreover, the positivity
272 of S_{1208}-specific cells was significantly lower than that of S_{448}-specific cells until after
273 the first shot; however, they became comparable after the second shot (Figure S6C).
274 Then, we performed TCR-seq on S_{448}- or S_{1208}-specific CD8+ T cells sorted from the
275 samples after the vaccinations (P2, P3, and P8) and identified S_{448}- or S_{1208}-specific
276 clonotypes ("Tetramer-TCRseq," Figure S6D). Furthermore, for each participant, we
277 determined whether the vaccine-induced S_{448}- or S_{1208}-specific T-cell responses were
278 observed (S_{448}- or S_{1208}-responders, Figure S6D). Among nineteen participants in whom
279 S_{448}-specific clonotypes were detected, seven were classified as S_{448}-responders, while
280 twelve were not (Figure 6D and Figure S6E). All nine participants in whom S_{1208}-
281 specific clonotypes were detected were S_{1208}-responders (Figure 6D). We focused on the
282 S_{448}- and S_{1208}-responder participants ("respondent") in the following section. In these
283 respondents, the total frequency of S_{448}- and S_{1208}-specific clonotypes increased after the
284 first shot and peaked after the second and third shots. At the peak of their response, the
285 total frequency of S_{1208}-specific clonotypes surpassed that of S_{448}-specific ones (Figure
286 S6F).
287 Finally, we examined whether the intra-epitope replacement of clonotypes was observed
288 for S_{448} and S_{1208}. S_{448}- and S_{1208}-specific clonotypes were classified into 1st, 2nd, dual,

289 and 3rd responders, and the total frequency of these responder clonotypes was calculated
290 for each participant, as in Figure 1 (Figure 6E and Figure S6G). Among S_{1208}-specific
291 clonotypes, 2nd and dual responders were observed in more than half of the respondents
292 (Figure 6E, thick line). Moreover, the total frequency of S_{1208}-specific dual responders
293 tended to be higher than 2nd responders after the first shot, while S_{1208}-specific 2nd
294 responders tended to surpass the dual responders after the second shot (Figure 6F).
295 These results are consistent with the replacement of clonotypes specific for the Spike
296 epitope S_{1208}. On the other hand, as for S_{448}-specific clonotypes, only 2nd responder
297 clonotypes were observed in more than half of the respondents, while dual and 3rd
298 responders were rare, and 1st responders were not observed (Figure S6G).
299

300 **Clonal replacement during mRNA vaccination occurs between and within Spike**
301 **epitopes**

302 TCRs recognizing the same pMHC often share conserved sequence motifs[35]. Based on
303 this property, we identified clonotypes specific for Spike epitopes for which pMHC
304 tetramer had been prepared (S_{448} and S_{1208}), and also clonotypes specific for other Spike
305 epitopes. From our original data of Tetramer TCR-seq and the public database of Spike-
306 specific TCRs[36,37], shared TCR sequence motifs of Spike-specific clonotypes were

307 constructed using tcrdist3 pipeline (Figure 7A)[38]. Then, we searched for T cell
308 clonotypes possessing the Spike-specific TCR motifs, based on the participants' HLA
309 alleles (Figure 7A). Through this TCR motif analysis, we identified clonotypes specific
310 for two Spike epitopes (S_{269}-A02:01 and S_{919}-B15:01), in addition to two epitopes used
311 in Tetramer TCR-seq (S_{448}-A24:02 and S_{1208}-A24:02). Spike-specific clonotypes
312 identified by TCR motif analysis were overlapped with those identified by Tetramer
313 TCR-seq (Figure S7A), and there were no clonotypes to which different specificities
314 were assigned between TCR motif analysis and Tetramer TCR-seq. On the other hand,
315 the overlap between clonotypes with Spike-specific TCR motifs and AIM^+ clonotypes
316 was negligible (Figure S7B), suggesting that the Spike epitopes used in TCR motif
317 analysis were presented to T cells less efficiently in our AIM assay with Spike peptide
318 pool.
319 We then quantified the temporal kinetics of T-cell responses specific to the four Spike-
320 epitopes by TCR motif analysis. Among these four Spike-epitopes, S_{919}-B15:01 was
321 most conserved between other human coronaviruses, while S_{448}-A24:02 was least
322 conserved and most unique to SARS-CoV-2 (Figure S7C). We observed that the
323 temporal kinetics of the Spike-specific T-cell response differed between these epitopes
324 (Figure 7B): S_{448}- and S_{1208}-specific responses were induced after the first shot and

325 peaked after the second and third shots, as observed in Tetramer TCR-seq analysis. The
326 S_{269}-specific response also peaked after the second and third shots, while induction after
327 the first shot was not observed (Figure 7B). The S_{919}-specific response peaked after the
328 first shot, but was not induced after the second and third shots (Figure 7B).
329 Furthermore, the total frequency of S_{919}-specific clonotypes was significantly higher
330 than S_{1208} and S_{269} after the first shot, while this was inverted after the second and third
331 shots (Figure S7D). These results suggest that inter-epitope replacement of vaccine-
332 responding clonotypes can occur between S_{919} and S_{269} in HLA-B15:01^{+} A02:01^{+}
333 participants, and between S_{919} and S_{448} or S_{1208} in HLA-B15:01^{+} A24:02^{+} participants.
334 However, we could not observe an example of the inter-epitope replacement within a
335 single participant in our cohorts.
336 Furthermore, we classified Spike-specific clonotypes into 1st, 2nd, dual, and 3rd
337 responders to examine whether the intra-epitope replacement of clonotypes was
338 observed. Among S_{269}- and S_{919}-specific clonotypes, only 2nd and 1st responders were
339 observed in more than half of the respondents, respectively (Figure S6E and F). On the
340 other hand, 1st and 2nd responders among S_{448}-specific clonotypes, and 2nd and dual
341 responders among S_{1208}-specific clonotypes were observed in more than half of the
342 respondents (Figure 7C, thick line). As for S_{448}-specific clonotypes, the total frequency

343 of 1st responders tended to be higher than 2nd responders after the first shot, while 2nd
344 responders were significantly more abundant than 1st responders after the second shot
345 (Figure 7D). Similarly, as for S_{1208}-specific clonotypes, the total frequency of dual
346 responders tended to be higher than that of 2nd responders after the first shot, while 2nd
347 responders tended to be more abundant than dual responders after the second shot
348 (Figure 7E). Moreover, we observed replacement between 1st and 2nd responders in four
349 of eight S_{448}-respondents and between dual and 2nd responders in three of twelve S_{1208}-
350 respondents (Figure S7H and G). These results provide examples of intra-epitope
351 replacement of vaccine-responding clonotypes within Spike epitopes S_{448} and S_{1208}.
352 In summary, temporal tracking of Spike-specific clonotypes using TCR motif analysis
353 demonstrated that the replacement of vaccine-responding clonotypes can occur within a
354 Spike epitope, which does not require the differences in the target epitope between the
355 1st and the 2nd responder clonotypes.
356

357 **Discussion**

358 Through a longitudinal TCR repertoire analysis combined with an AIM assay, single-
359 cell TCR sequencing, and TCR motif analysis, we demonstrated that clonotypes newly
360 expanded after the second vaccination largely replaced the clonotypes that had

361 responded to the first shot. Moreover, although these 2nd responder clonotypes expanded
362 again with an effector memory phenotype, their diversity was further skewed after the
363 third shot, and they were partially replaced by the mobilization of the 3rd responders.
364 Furthermore, this replacement of vaccine-responding clonotypes can occur not only
365 between, but also within, clones specific for Spike epitopes. These data are consistent
366 with a clonal replacement model of T-cell memory responses under repetitive antigen
367 challenges in humans receiving SARS-CoV-2 mRNA vaccinations[18].
368 To fully understand T cell clonal replacement following repeated mRNA vaccination, it
369 is essential to clearly define the nature of 1st, 2nd, and dual responders. Secondary
370 memory T cell responses are faster and more aggressive than the primary responses
371 being medicated by naïve cells[39]. Based on this notion, we consider the 2nd responder
372 clonotypes as those that exerted the primary response after the first shot and recall
373 response after the second shot. In our analysis, the primary response of most of the 2nd
374 responders was not detected after the first shot. We suppose this is because the cell
375 count of 2nd responders at the sampling point after the first shot is too small to detect
376 through our bulk TCR-seq at P2, day 7 after the first shot.
377 In contrast, the dual and the 1st responder clonotypes expanded quickly and vigorously
378 after the first shot, which appeared closer to a recall response than a primary one.

379 Memory T cells cross-reactive to SARS-CoV-2 and 'common cold' coronaviruses
380 (CCCoV) likely existed in many individuals before the COVID-19 pandemic[40–43].
381 Therefore, 1st and dual responders may be "pre-existing memory" clonotypes that have
382 been primed by CCCoV before the pandemic and exerted recall response by recognizing
383 the SARS-CoV-2 Spike after the first shot. We further propose that their weak response
384 after the second and third shot is that they differentiate into secondary memory with a
385 weaker proliferative ability[44–46]. This is in line with the report that the contribution of
386 $CD4^+$ cross-reactive T cells to the Spike-reactive T-cell pool is minimal after
387 vaccination against SARS-CoV-2[47].
388 Consistent with this interpretation for 1st, 2nd, and dual responders, we propose that the
389 T-cell response to S_{919}, the most conserved Spike epitope analyzed in this study, was
390 exerted by 1st responder clonotypes. Moreover, the response to the less conserved S_{269}
391 and S_{1208} epitopes was mainly exerted by 2nd responders. On the other hand, the 1st
392 responder clonotypes were broadly observed in S_{448}-specific clonotypes, contrary to the
393 fact that S_{448} was least conserved among the four Spike epitopes, implying that pre-
394 existing memory to SARS-CoV-2 S_{448} was less likely to exist. To explain this, we
395 propose that there are pre-existing memory T cells that recognize epitopes similar to
396 S_{448} derived from pathogens other than human coronavirus. Further studies are needed

397 to prove the relationship between 1st and dual-responder clonotypes and pre-existing
398 memory T cells.
399 Determining whether clonal replacement through mRNA vaccination occurs between
400 different Spike epitopes (inter-epitope replacement), or even within, a single Spike
401 epitope (intra-epitope replacement) is an important step to understand the mechanism of
402 clonal replacement. In the case of anti-Spike B cell responses following mRNA
403 vaccination, differences in the response kinetics were reported between the target: the
404 faster response to the S2 domain occurring after the first shot, which is cross-reactive to
405 CCCoV, and the slower response to the S1 domain occurring after the second shot[48].
406 Like the B-cell response, our analysis identified a differential kinetics of Spike-specific
407 T-cell responses between epitopes (i.e., response induced only after the first shot (S_{919}),
408 only after the second shot (S_{269}), or both after the first and second shot (S_{448} and S_{1208})).
409 This result supports the inter-epitope replacement model, possibly due to a shift of
410 immunodominance in Spike epitopes through vaccination. Cases of inter-epitope
411 replacement within a single participant were not observed, but might be found if we
412 analyze larger cohorts with various combinations of HLA alleles, or if the Spike-
413 specific TCR database was expanded to cover more diverse Spike epitopes. On the other
414 hand, replacement between 2nd responders and 1st or dual responders was observed

415 within the same epitopes (S_{448} and S_{1208}) even in the same individual, which supports
416 the inter-epitope replacement model. This observation implies the coexistence of two
417 groups of clonotypes within a single Spike epitope: pre-existing memory clonotypes
418 cross-reactive to CCCoV and newly expanded clonotypes specific to SARS-CoV-2.
419 This complex nature of T-cell clonal responses within a single Spike epitope should be
420 addressed through more intensive analysis of epitope-specific T cells and the
421 identification of TCR motifs related to the responding patterns of clonotypes.
422 The third- and fourth-vaccination induces a more robust humoral and cellular immune
423 response to SARS-CoV-2 than the second-vaccination[49,50], and increases the protection
424 against SARS-CoV-2 infection, including the Omicron variant[51,52]. As of April 2023,
425 nearly 70 % and 50 % of the population in Japan have undergone more than three and
426 four shots of vaccination, respectively. Our TCR repertoire analysis after the third
427 vaccination demonstrated that the 2nd responders were still dominant among vaccine-
428 responding clonotypes and not significantly replaced by the 3rd responders. However,
429 after the third shot, 2nd responders exhibited a more differentiated phenotype, and their
430 diversity was significantly decreased compared to that after the second shot, resulting in
431 the skewing of the 2nd responders' repertoire. The key question remains whether the
432 diversity of 2nd responders continued to decrease after four or more shots and whether

433 3rd or 4th responders can compensate for it. If this is the case, strategies may be needed
434 to maintain the diversity of vaccine-responding clonotypes by replenishing the novel
435 expanding ones under repetitive vaccination. Extending our TCR repertoire analysis
436 after the fourth vaccination would provide critical information for optimizing the
437 protocol for mRNA vaccination.
438 As far as we know, this study provided the first bulk TCR repertoire analysis dataset on
439 more than 30 participants covering the entire time course of mRNA vaccinations (from
440 the first shot to six months after the third shot). Moreover, the sampling time point is
441 uniform across the participants, enabling the comprehensive analysis of the kinetics of
442 T-cell clonotype expansion following vaccination. In addition to the analysis of the
443 responding pattern of clonotypes, the comparison of the rate of contraction between
444 vaccine-responding clonotypes would provide important information for understanding
445 T-cell responses induced by mRNA vaccination. Moreover, the majority of the
446 participants in our cohort reported neither clear infection history nor signs of past
447 SARS-CoV-2 infection. Thus, our data reflect the effect of vaccination on T-cell
448 repertoire more accurately. One defect in our dataset, however, is that the sampling
449 point after the first vaccination (P2, day 7 after the first shot) was a few days earlier than
450 the peak of T-cell responses to the first shot (around day 9-12)[53]. This earlier sampling

451 can lead to an underestimation of the T cell response after the first shot: recall response
452 of 1st and dual responder clonotypes, and the primary response of 2nd responders.
453 However, an expansion of Spike-specific T-cell clonotypes (to S_{919}, S_{448}, and S_{1208}) was
454 observed at P2, confirming that this time point is not too early to detect vaccine-induced
455 T-cell responses.
456 An important question is whether the clonal replacement we demonstrated in this study
457 is specific to the mRNA vaccination or is common to the other types of vaccination or
458 natural infections. We initially reported the clonal replacement in the antigen delivery
459 systems using plasmid and viral vectors[18]. In addition, in the case of vaccination to
460 yellow fever virus (YFV), the clonal composition of YFV-specific $CD4^+$ T cells is
461 reshaped by a single vaccination[54], and the vaccine-responding $CD8^+$ clones are also
462 turned over between the prime and boost shots[55]. On the other hand, the trivalent
463 influenza vaccination induces a response by T cells mainly recruited from the pre-
464 existing memory clones[56]. This inconsistency in whether the clonal replacement occurs
465 may be attributed to the type of vaccine (mRNA or live attenuated versus inactivated) or
466 the novelty of the antigen (SARS-CoV-2 or YFV versus seasonal flu). Further study is
467 needed to elucidate the requirements for clonal replacement after vaccination. In
468 addition, considering that natural SARS-CoV-2 infection generates tissue-resident

469 memory T cells (T_{RM}) in the lung[57], the replacement of antigen-specific clonotypes in
470 blood after re-infection, if it occurs, may be associated with the re-distribution of older
471 clonotypes from the blood to peripheral tissues and their differentiation to T_{RM}.
472 Collectively, along with the temporal analysis of blood T cell repertoire as done in the
473 current study, a systemic analysis of the T cells in peripheral tissues is essential to
474 understand the kinetics of T-cell clonal response by natural infection.
475 In summary, we demonstrated the replacement of memory T-cell clones during SARS-
476 CoV-2 mRNA vaccination. In contrast to humoral immunity mediated by memory B
477 cells and long-lived plasma cells, where the memory response to the first viral variant
478 encountered in childhood is preferentially employed even after the challenge of other
479 variants in adults (original antigenic sin)[58,59], T cells appear to be able to reshape the
480 memory population after repetitive challenges. This "re-writability" of T cell
481 immunological memory may enable them to effectively generate responses to variant
482 strains of the virus.
483

484 **Methods**

485 **Study design**

486 38 healthcare workers (≥20 years old) at Nara Medical University in Japan who had

487 received the first shot of Pfizer-BNT162b2 vaccine between 10 March and 30 March
488 2021 were invited to participate as volunteers in the study. The Nara Medical University
489 Ethics Committee approved the study (No. 2954 and 3168). In this cohort, no one
490 reported a SARS-CoV-2 infection history before or during the initial sampling period.
491 Four and two participants showed signs of past SARS-CoV-2 infection before the first
492 and third vaccination, respectively (inferred by the anti-Nucleoprotein (N) antibody
493 titer). Peripheral blood samples were collected before receiving the first dose (P1), 1
494 week after the first shot (P2), 1 week (P3), 1 month (P4), 3 months (P5), and 6 months
495 (P6) after the second shot, and 1 week (P8), 1 month (P9), 3 months (P10), and 6
496 months (P11) after the third shot. One participant (ID18) was not sampled at P11
497 because they had received the fourth vaccination before this time point. Participants
498 were asked to report the following adverse events after each vaccination: pain, swelling,
499 heat, fever, fatigue, headache, chills, joint pain, and muscle pain. PBMCs were isolated
500 from whole blood with BD vacutainer CPT tubes (BD reagents used in this study are
501 summarized in Supplementary Table S3), resuspended in CELLBANKER 1 (Takara),
502 and stored at -80°C. The detailed study design was described in Kitabatake et al.[19].

503 **Study approval**

504 The study was conducted in accordance with the Declaration of Helsinki and Good

505 Clinical Practice Guidelines, following approval by the ethics board in each institution.

506 All study participants provided written informed consent.

507 **Evaluation of anti-SARS-CoV-2 antibodies**

508 Serum samples were tested for antibody titer against RBD of SARS-CoV-2 ancestral

509 strain, SARS-CoV-2 Omicron spike variant protein, and nucleocapsid protein of SARS-

510 CoV-2 ancestral strain, were tested using RayBio COVID-19 S1 RBD protein Human

511 IgG ELISA Kit (RayBiotech), RayBio COVID-19 Omicron Spike Variant Human IgG

512 ELISA Kit (RayBiotech), and RayBio COVID-19 N protein Human IgG ELISA Kit

513 (RayBiotech) per the manufacturer's instructions, respectively.

514 **T-cell isolation from PBMCs**

515 $CD4^+$ and $CD8^+$ T cells were magnetically isolated from PBMC. PBMC were thawed by

516 warming frozen cryovials in a 37°C water bath. Cells were stained for 20 minutes at

517 4°C with 1st antibody mix (Antibody Mix 1 in Supplementary Table S4). After washing

518 with MACS buffer [0.5% BSA (Nacalai), 2 mmol/L EDTA (NIPPON GENE) in PBS

519 (Nacalai)], Cells were stained for 20 minutes at 4°C with 2nd antibody mix; BD IMag

520 anti-PE Magnetic Particles-DM (Clone E31-1459, BD) and anti-APC-Biotin (clone

521 APC003, BioLegend). Then, the cell suspension was diluted with MACS buffer and set

522 on a magnet plate (DynaMag96SideSkirted, Veritas). The positive fraction was collected

523 as $CD4^+$ T cells. The negative fraction was stained with BD IMag Streptavidin Particles

524 Plus-DM (BD) for 20 minutes at 4°C. Then, the cell suspension was diluted with MACS

525 buffer and set on a magnet plate. The positive fraction was collected as $CD8^+$ T cells

526 and B cells. The counts of $CD4^+$ T cells, $CD8^+$ T cells, and B cells were determined

527 using Flow-Count fluorospheres (Beckman) and a Cytoflex flow cytometer (Beckman)

528 and FlowJo software (version 10.8.1; BD Biosciences, software and algorithms used in

529 this study are summarized in Supplementary Table S5).

530 **HLA genotyping**

531 Genome DNA was extracted from PBMC using Geno Plus Genomic DNA Extraction

532 Miniprep System (VIOGENE) using serum and animal cell protocol with RNase A

533 treatment. DNA was quantified on the NanoDrop (Thermo Fisher Scientific). HLA

534 genotyping was performed on genome DNA using the reverse sequence-specific

535 oligonucleotide probe Luminex method at HLA Laboratory (Kyoto, Japan).

536 **AIM assay and sorting Spike-reactive T cells.**

537 AIM assay was performed on PBMC samples collected at P2, P3, and P8. PBMC were

538 thawed by warming frozen cryovials in a 37°C water bath and resuspended in 10mL of

539 in Culture Medium (CM) [10% fetal bovine serum (MP Bio Japan), 1% HEPES

540 (Nacarai) and 1% penicillin/streptomycin (Nacarai) in RPMI-1640 medium (Nacarai)].

541 Cells were resuspended in 1mL of CM, then plated in 24-well plates and incubated
542 overnight (about 16 hours) in an incubator at 37°C, with 5% CO_2. After incubation, cells
543 were then stimulated for 24 hours in stimulation medium [CM with BD FastImmune
544 CD28/CD49d Costimulatory Reagent (final x100, BD Biosciences) and anti-human
545 CD40 (final concentration of 0.5µg/mL, clone HB14, BioLegend)] with or without
546 PepTivator SARS-CoV-2 Prot_S Complete (final concentration of 1 mg/mL, Miltenyi).
547 20 hours post-stimulation, an anti-CD107a-FITC antibody (final concentration of
548 5µg/mL, clone H4A3, BioLegend) was added to the culture. After four hours, cells were
549 washed in PBS supplemented with 10% FBS (10% FBS/PBS). Cells were stained for 20
550 minutes at 4°C with antibody mix 2 (Supplementary Table S4). Cells were washed once
551 in 10% FBS/PBS. AIM^+ non-naïve $CD4^+$, AIM^- non-naïve $CD4^+$, AIM^+ non-naïve
552 $CD8^+$, and AIM^- non-naive $CD8^+$ cells were sorted using FACS Aria II or Aria III (BD
553 Biosciences) and FACSDiva software (BD Biosciences, v8.0.1). AIM^+ $CD4^+$ T cells
554 were defined by dual expression of CD69 and CD40L. AIM^+ $CD8^+$ T cells were defined
555 by expression of either CD107a or CD137. Nonviable cells were excluded from the
556 analysis based on forward and side scatter profiles and propidium iodide staining (PI,
557 Sigma-Aldrich). Data were analyzed using FlowJo software.

558 **Sample preparation for single-cell analysis**

559 PBMC thawed as described above were resuspended with Cell Staining Buffer
560 (BioLegend) supplemented with Human TruStain FcX. After 2-3 minutes, 2x AbSeq
561 master mix of Immune Discovery Panel (BD Biosciences) prepared as the provider's
562 protocol was added to the cell suspension and stained for 15 minutes on ice. Then,
563 antibody mix 3 (Supplementary Table S4) with Sample Tag oligonucleotide-conjugated
564 antibodies (Single-Cell Multiplexing Kit, BD Biosciences) was added to the cell
565 suspension and left on ice for 15 minutes for staining. The correspondence between
566 samples and Sample Tags used was described in Supplementary Table S2. Stained cells
567 were washed with Cell Staining Buffer. Then non-naive $CD4^+$ and $CD8^+$ cells (ID2 and
568 ID27) or only non-naive $CD8^+$ cells (ID10, ID19, ID22, ID31, and ID35) were sorted
569 using FACS Aria II or Aria III and FACSDiva software (v8.0.1). Nonviable cells were
570 excluded from the analysis based on forward and side scatter profiles and PI staining.
571 Data were analyzed using FlowJo software (version 10.8.1).

572 **Tetramer staining and sorting Spike-specific T cells.**

573 S_{448} and S_{1208} peptides were purchased from GenScript. Peptides-MHC class I tetramers
574 for SARS-CoV-2 Spike epitopes (S_{448} and S_{1208}) were generated by QuickSwitchTM
575 Quant HLA-A*24:02 Tetramer Kit-BV421, and -PE (MBL), respectively, according to
576 the manufacturer's protocol. The rate of peptide exchange was reported to be more than

577 95% in our previous report[32]. Thawed PBMCs were treated with a protein kinase

578 inhibitor, Dasatinib (50 nM, AdooQ), for 30 min at 37 °C, and Human TruStain FcX for

579 5 minutes at room temperature. Then, PBMCs were stained with tetramers for 30

580 minutes at room temperature. After tetramer staining, cells were stained for antibody

581 mix 4 (Supplementary Table S4) for 20 minutes at room temperature. After washing

582 twice with FACS buffer, $CD8^+$ $tetramer^+$ cells were sorted using FACS Aria II or Aria

583 III and FACSDiva software (v8.0.1). Nonviable cells were excluded from the analysis

584 based on forward and side scatter profiles and PI staining. Data were analyzed using

585 FlowJo software (v10.8.1).

586 **Library preparation and sequencing for TCR repertoire analysis**

587 TCR sequencing libraries for next-generation sequencing were prepared according to

588 the previous report[60]. In brief, mRNA in T-cell lysates were captured by incubating with

589 10 μL of Dynabeads M270 streptavidin (Thermo Fisher Scientific) bound to 2.5 pmol of

590 BioEcoP-dT25-adapter primers for 30 minutes at room temperature under gentle

591 rotation. mRNA-trapped beads were suspended in 10 μL of RT mix and incubated for

592 60 min at 42ºC to perform reverse transcription (RT) and template-switching. The

593 composition of the RT mix was as follows; 1× First Strand buffer (Thermo Fisher

594 Scientific), 1 mM dNTP (Roche), 2.5 mM DTT (Thermo Fisher Scientific), 1 M betaine

595 (Sigma-Aldrich), 9 mM MgCl2 (NIPPON GENE), 1 U/μL RNaseIn Plus RNase
596 Inhibitor (Promega), 10 U/μL Superscript II (Thermo Fisher Scientific), and 1 μM of i5-
597 TSO. To amplify the TCR cDNA containing complementarity determining region 3
598 (CDR3), nested PCR of the TCR locus was performed using KAPA Hifi Hotstart
599 ReadyMix (KAPA Biosystems), followed by the purification of PCR product using an
600 AM Pure XP kit (Beckman Coulter) at a 0.7:1 beads-to-sample ratio. The third PCR was
601 performed to amplify TCR libraries and add adaptor sequences for the next-generation
602 sequencer. The third-PCR products were purified as described for the second PCR. Final
603 TCR libraries, whose lengths were about 600 base pairs, were quantified using a KAPA
604 SYBR Fast qPCR Kit (KAPA Biosystems), and size distribution was analyzed by
605 Microchip Electrophoresis System MultiNA (Shimadzu). TCR libraries were sequenced
606 using an Illumina Novaseq 6000 S4 flowcell (67 bp read 1 and 140 bp read 2)
607 (Illumina) using NovaSeq 6000 S4 Reagent Kit v1.5 (200 cycles, Illumina). Only read2
608 contained the sequence regarding the definition of T-cell clones. Oligonucleotides and
609 reaction conditions for library preparation were summarized in Table S6 and S7,
610 respectively.
611 For tetramer TCR-seq, the libraries were prepared on samples with (i) more than 100
612 tetramer^{+} cells and (ii) the proportion of tetramer^{+} cells was more than 0.1% in CD8^{+} T

613 cells. S_{1208}-tetramer^{+} samples with a high background (ID22) were excluded from the

614 analysis.

615 **Library preparation and sequencing for single-cell analysis**

616 Single-cell sequencing libraries were prepared according to the previous report[60]. Live

617 cells were stained with Calcein AM (Nacalai) and counted using Flow-Count

618 fluorospheres and a Cytoflex flow cytometer. About 25,000 - 30,000 labeled cells were

619 loaded on a BD Rhapsody cartridge (BD) and processed using BD Rhapsody™

620 Cartridge Reagent Kit (BD) following the manufacturer's instructions. Single-cell

621 mRNA, AbSeq barcodes, and Sample Tag barcodes were captured by BD Rhapsody

622 beads coated with poly(T) oligonucleotide with a unique cell barcode and molecular

623 barcode on each bead. Single-cell cDNA synthesis was performed using BD Rhapsody

624 cDNA Kit (BD) following the manufacturer's protocol. Targeted mRNA, TCRseq, and

625 Abseq Index libraries were prepared using Immune Response Panel HS (BD) according

626 to the manufacturer's instructions with the following modifications. (1) We used the

627 original set of primers for TCR amplification, as summarized in Table S6. (2) We

628 performed additional PCRs to introduce a unique dual index for sequencing (3rd PCR

629 for mRNA and TCR), as described in Table S8. (3) We used the ProNex Size-Selection

630 DNA Purification System (Promega) to purify PCR products, as summarized in Table

631 S8. Amplified libraries were quantified using a KAPA SYBR Fast qPCR Kit (KAPA
632 Biosystems), and size distribution was analyzed by Microchip Electrophoresis System
633 MultiNA (Shimadzu). Targeted RNAseq, TCRseq, and AbSeq libraries were sequenced
634 on an Illumina Novaseq 6000 S4 flowcell (67 bp read 1 and 140 bp read 2) using
635 NovaSeq 6000 S4 Reagent Kit v1.5 to a depth of approximately 20,000 reads, 7,000
636 reads, and 10,000 reads per cell, respectively.

637 **Data processing of TCR sequencing reads**

638 Data processing of TCRseq was performed as previously reported[60]. Briefly, Adapter
639 trimming and quality filtering of sequencing data were performed using Cutadapt-3.2[61]
640 and PRINSEQ-0.20.4[62]. Sequencing data were processed by MiXCR-3.0.5[63]. In
641 MiXCR, filtered reads were aligned to reference mouse TCR V/D/J sequences
642 registered in the international ImMunoGeneTics (IMGT) information system. The
643 parameters used in MiXCR are summarized in Supplementary Table S9. The Variable
644 (V) and Joining (J) segments of TCRs were represented in IMGT gene nomenclature. T-
645 cell clones were determined as TCR reads with the same TCR V segment, J segment,
646 and CDR3 nucleotide sequence.

647 For bulk TCRseq data, we regarded the $CD4^+$-$CD8^+$ overlapping clones in the same
648 participant as contamination during T-cell isolation from PBMC because $CD4^+$ and

649 $CD8^+$ T-cell repertoire are mutually exclusive[64]. Thus, these overlapping clones were
650 categorized into either $CD4^+$ or $CD8^+$ according to their dominance in $CD4^+$ and $CD8^+$
651 repertoire using VDJtools-1.2.1[65]. Inter-sample contamination within samples using the
652 same UDIs was excluded by the "Decontaminate" function of vdjtools with the
653 parameter "-r 10". The sequencing reads of bulk TCR-seq samples were normalized to
654 100,000 reads by the “DownSample” command of VDJtools-1.2.1[65]. To preserve the
655 minor clonotypes, we performed the normalization ten times and pooled these down-
656 sampled repertoire data for each sample by the “JoinSamples” command of VDJtools-
657 1.2.1. The sequencing reads of AIM TCR-seq or tetramer TCR-seq samples were
658 normalized to 16 times the cell count (AIM assay-TCRseq data) in each sample by the
659 “DownSample” command of VDJtools-1.2.1[65], and TCR clones with 15 or fewer reads
660 were regarded as sampling noise and removed from the dataset[64].

661 **Identifying vaccine-responding clonotype using bulk TCR-seq dataset**

662 Clonotypes that significantly expanded after vaccination (vaccine-responding
663 clonotype) were identified by differential abundance analysis using the beta-binomial
664 model[20]. Before performing differential abundance analysis on clonotype frequency, the
665 total count of bulk TCRseq data was adjusted to 100,000. Then, vaccine-responding and
666 vaccine-increased clonotypes are defined for each vaccination (P2, P3, or P8).

667 Clonotypes are regarded as “responded to vaccination” when (i) they had a significant
668 increase in their frequency and (ii) their frequency was increased more than two-fold
669 between before and after the vaccination. Vaccine-responding clonotypes were also
670 identified between the baseline (P0) and after the second shot (P3). In addition,
671 clonotypes are regarded as “increased after vaccination” when (i) their frequency was
672 increased between before and after the vaccination, (ii) their frequency was increased
673 more than two-fold between the baseline (P1) and after the vaccination, and (iii) their
674 frequency was more than 0.0025% after the vaccination. Finally, Clonotypes that did
675 not meet the requirements for vaccine-responding or vaccine-increased clonotypes were
676 regarded as “did not respond to vaccination.” The beta-binomial model incorporates
677 time-dependent variance of clonotype frequency using normal peripheral blood T cell
678 repertoire variance over two weeks[20].

679 **Identifying 1st, 2nd, dual, and 3rd responder clonotypes in bulk TCR-seq dataset**

680 1st responder clonotypes were defined as clonotypes that responded to the first shot, but
681 did not respond to the second one. 2nd responder clonotypes were defined as clonotypes
682 that responded to the second shot while did not respond to the first shot. Dual responder
683 clonotypes were defined as clonotypes that responded or increased after the first and
684 second shots, and that responded between the baseline (P0) and after the second shot

685 (P3). 3rd responder clonotypes were defined as clonotypes that were not detected before

686 the third shot and responded to the third shot. We excluded clonotypes whose frequency

687 was over 0.01% at baseline from 1st, 2nd, and dual responders.

688 **Identifying Spike-reactive clonotypes through AIM TCR-seq dataset.**

689 Spike-reactive clonotypes were identified using the dataset of AIM TCR-seq as in

690 Figure 2B. "AIM^+ enrichment ratio" was calculated for each clonotype as (frequency in

691 AIM^+ repertoire + 5×10^{-6}) / (frequency in AIM^- repertoire + 5×10^{-6}). Clonotypes with

692 an AIM^+ enrichment ratio over 16 were defined as Spike-reactive clonotypes, and their

693 frequency was tracked in the bulk TCR-seq dataset.

694 **Calculation of clonality or evenness of TCR repertoire**

695 The 1 - Pielou index was used to evaluate the clonality of TCR repertoire, which was

696 calculated using the formula $1 - \sum_{i=1}^{n} p_i \log_e(p_i) / \log_e(n)$, where p_i is the frequency

697 of clone *i* for a sample with *n* unique clones. The DE90 index was used to evaluate the

698 evenness of the TCR repertoire, which was calculated as the ratio between the number of

699 clonotypes whose cumulative frequency is 90% and the total number of clonotypes in the

700 repertoire[66].

701 **Identifying Spike-specific clonotypes through tetramer TCR-seq dataset.**

702 S_{448}- and S_{1208}-specific clonotypes were identified using the dataset of tetramer TCR-

703 seq and bulk TCR-seq as in Figure S6D. "Tetramer^{+} enrichment ratio" was calculated

704 for each clonotype as (frequency in tetramer^{+} repertoire + $5x10^{-6}$) / (maximum

705 frequency in bulk TCR-seq datasets from P1 to P11 + $5x10^{-6}$). Clonotypes with a

706 tetramer^{+} enrichment ratio over 16 were defined as S_{448}- or S_{1208}-specific clonotypes,

707 and their frequency was tracked in the bulk TCR-seq dataset. Then, epitope-responsive

708 participants were defined as those whose total frequency of epitope-specific clonotypes

709 was (i) more than 0.05% and (ii) 5-fold increased after the first or the second shot (red).

710 **Identifying Spike-specific clonotypes through TCR motif analysis using tcrdist3**

711 To identify Spike-specific clonotypes through TCR motif analysis in our dataset, we

712 utilized the framework introduced in Mayer-Blackwell et al.[38]. In this framework, we

713 first formed meta-clonotypes (groups of TCRs that were biochemically similar) of

714 Spike-specific TCRs. Then we searched TCRs conformant to the definition of the meta-

715 clonotypes (meta-clonotype conformant TCRs).

716 Spike-specific meta-clonotypes are formed using Spike-specific TCR sequences from

717 two public databases (vdjdb and immune epitope database: IEDB) and our tetramer

718 TCR-seq datasets as an input. In this step, the TCR sequence motif and optimal radii

719 were estimated for each meta-clonotype at which background TCRs were detected at a

720 frequency of $< 10^{-5}$. Then, Spike-specific TCRs were searched in our dataset using these

721 Spike-specific meta-clonotypes and meta-clonotypes reported in Mayer-Blackwell et
722 al.[38], which were identified from MIRA Spike antigen stimulation assay dataset[37] with
723 significant association for HLA-restricted epitopes. In this step, the query list of Spike-
724 specific meta-clonotypes was generated for each participant by selecting meta-
725 clonotypes whose epitope-presenting HLA allele matched the participant's HLA
726 genotypes. The frequency of Spike-specific clonotype was tracked in bulk TCR-seq
727 dataset, and epitope-responsive participants were defined as for the tetramer TCR-seq
728 data analysis.

729 **Data processing of scRNAseq reads**

730 Data processing of scRNAseq reads was performed as described in Shichino et al [67].
731 Adapter trimming of sequencing data was performed by using cutadapt 3.4[61]. Filtered
732 reads were chunked into 16 parts for parallel processing using Seqkit 0.15.0[68]. Filtered
733 cell barcode reads were annotated by Python script provided by BD with minor
734 modifications to be compatible with Python3.8. Associated cDNA reads were mapped to
735 reference RNA (build GRCh38 release-104) using bowtie2-2.4.2[69] by the following
736 parameters: -p 2 -D 20 -R 3 -N 0 -L 8 -I S,1,0.75 –norc –seed 656565 –reorder. Then,
737 cell barcode information of each read was added to the bowtie2-mapped BAM files, and
738 read counts of each gene in each cell barcode were counted by using mawk. The

resulting count data was converted to a genes x cells matrix file, and the knee-plot inflection threshold was detected using the DropletUtils package in R version 4.1.2[70]. In addition, we further estimate background beads using the emptyDrops formula in the DropletUtils package. Cells of total read count over inflection point were considered valid cells.

Data processing of sample tag reads

For sample tag data, adapter trimming of sequencing data was performed using cutadapt 3.4[61]. Filtered reads were chunked to 64 parts for parallel processing using Seqkit 0.15.0[68]. Filtered cell barcode reads were annotated using the Python script provided by BD with a minor modification to allow compatibility with Python3.8. Associated sample tag reads were mapped to known barcode fasta using bowtie2-2.4.2[69] with the following parameters: -p 2 -D 50 -R 20 -N 0 -L 14 -i S,1,0.75 –norc –seed 656565 –reorder –trim-to 3:40 –score-min L,-9,0 –mp 3,3 –np 3 –rdg 3,3.

The cell barcode information for each read was added to the bowtie2-mapped BAM files, and read counts of each Tag in each cell barcode were counted using mawk. The resulting count data were converted to a Tags x cells matrix file using the data.table package in R 3.6.3, and the top 1M cell barcodes were extracted. For the assignment of individual tags to cell barcodes, read counts of each tag in each valid cell barcode, defined

757 by the cDNA matrix, were extracted from the tag/cell barcode expression matrix.
758 Unassigned cell barcodes were labeled as "not-detected" cells. The sum of the total read
759 counts of each tag was normalized to the minimum sum count of each tags, and $\log_2$ fold-
760 change between first most tag counts and second most tag counts within each cell barcode.
761 Each cell barcode was ranked by the fold-change ascending order, and top N cells were
762 identified as doublets (N was calculated as theoretically detectable doublets calculated
763 using the Poisson's distribution based on the number of loaded cells, total Rhapsody well
764 number, and the number of tags used).

765 **Data processing of AbSeq reads**

766 For AbSeq data, adapter trimming of sequencing data was performed using cutadapt 3.4
767 [61]. Filtered reads were chunked into 64 parts for parallel processing using Seqkit 0.15.0
768 [68]. Filtered cell barcode reads were annotated by Python script provided by BD with
769 minor modifications to be compatible with Python3.8. Associated AbSeq reads were
770 mapped to known barcode fasta by using bowtie2-2.4.2[69] by the following parameters: -
771 p 2 -D 20 -R 3 -N 0 -L 8 -I S,1,0.75 –norc –seed 656565 –reorder–trim-to 3:39 –score-
772 min L,-9,0 –mp 3,3 –np 3 –rdg 3,3. Then, the cell barcode information of each read was
773 added to the bowtie2-mapped BAM files, and read counts of each AbSeq tag in each
774 cell barcode were counted using mawk. The resulting count data were converted to tags

775 x cells matrix file by using the data.table package in R version 4.1.2, and top 1M cell

776 barcodes were extracted.

777 **Correct batch effect in scRNAseq and AbSeq data**

778 scRNAseq/AbSeq data analysis was performed using the R software package Seurat

779 v4.0.1[71]. Expression data of targeted panel genes and surface proteins were converted to

780 the Seurat object. $CD4^-$ $CD8^+$ cells were extracted based on the expression level of CD4

781 and CD8 proteins determined by AbSeq. Then, expression data was log-normalized and

782 scaled using NormalizeData and ScaleData functions, respectively. For scRNAseq data,

783 the batch effect was corrected as in Stuart et. al.[72], using reciprocal principal component

784 analysis (PCA) in Seurat. Then, PCA was performed using RunPCA (the number of

785 calculated principal components (PCs) was 50). The enrichment of each PC was

786 calculated using the JackStraw and ScoreJackStraw function (num.replicate = 100), and

787 PCs that were significantly enriched ($p \leq 0.05$) were selected for further analysis. For

788 AbSeq data, genes unrelated to the phenotype of $CD8^+$ T cells (CD14, CD16, CD19,

789 CD3, CD4, CD8, CXCR5, IgD, and IgM) were excluded, then, the batch effect of

790 selected genes (CD27, CD28, CD56, CD62L, and CD161) were corrected using the

791 ADTnorm function in the package ADTnorm[73]. The expression data of the other genes

792 (CCR7, CD11c, CD25, CD45RA, CD127, CD134, CD137, CD183, CD196, CD272,

793 CD278, CD279, CXCR6, GITR, HLA-DR, and Tim3) was log-normalized using
794 NormalizeData function. After that, data scaling and PCR were performed using
795 ScaleData and RunPCA function.

796 **Cell clustering through integrative analysis of scRNAseq and AbSeq data**

797 Cell clustering was performed based on the weighted-nearest neighbor graph using
798 FindMultiModalNeighbors and FindClusters against the significant PCs of scRNAseq
799 and AbSeq[74]. The dimensional reduction was performed using RunUMAP based on the
800 nearest neighbor graph determined by FindMultiModalNeighbors. Marker genes of each
801 identified cluster were identified using the FindAllMarkers function (test.use="Wilcox",
802 min.pct=0.1, return.thresh=0.05). Clusters constituted with contaminant cells
803 determined by marker genes were excluded, and the above analysis procedure was
804 repeated.

805 **Transcriptional signature analysis in scRNAseq**

806 We computed the extent to which gene signatures were expressed in cells using
807 Seurat's "AddModuleScore" function. Signature genes related to the T-cell phenotypes
808 were obtained from the dataset published by Galleti et al.[75]. Effector and Cell cycle
809 signature genes were obtained based on the descriptions of Immune Response Panel HS.
810 Genes used for calculating signature scores are summarized in Supplementary Table S10.

811 **Data processing and analysis of scTCRseq**

812 Raw data from single-cell TCR sequencings were processed by the pipeline produced
813 by ImmunoGeneTeqs, Inc., as described previously[60]. Briefly, sequencing reads were
814 separated by cell barcode, then adapter trimming and quality filtering of sequencing
815 data were performed using cutadapt 3.4[61]. PCR and sequencing errors were corrected by
816 lighter v1.1.2[76] with the following parameters: -newQual 25 -maxcor 4 -K 20. Error-
817 corrected sequence reads were processed by MiXCR[63] to generate the list of TCRα or
818 TCRβ sequences for each cell barcode, using reference human TCR V/D/J sequences
819 registered in the international IMGT information system. Quality filtering of cell
820 barcodes was performed with the following criteria: (1) more than 32 TCR reads were
821 detected. (2) the proportion of the most frequent TCR sequence in cell barcodes was
822 over 0.6. (3) the cell barcode was annotated to the T cell cluster in scRNAseq/AbSeq
823 analysis. Parameters used in MiXCR are summarized in Supplementary Table S11.
824 Finally, the most frequent sequence of TCRα and TCRβ was adopted and paired in each
825 cell barcode. Identified TCRα or TCRβ sequence was imported into the meta.data
826 matrix in the Seurat object of scRNAseq/AbSeq data based on the cellular barcode
827 identities. T-cell clones were determined as cells with the same TCRβ sequence defined
828 by the V segment, J segment, and CDR3 nucleotide sequence. The frequency of each

829 clone was calculated as the proportion of cells belonging to the clone in all T cells

830 whose TCRβ sequence was assigned.

831 **Calculating the TCR repertoire meta-parameter for correlation analysis**

832 Co-regulated TCR repertoire parameters (“repertoire meta-parameters") were

833 independently determined for $CD4^+$ and $CD8^+$ T cells. First, a Spearman correlation

834 coefficient was calculated for all pairs of repertoire parameters; then, repertoire

835 parameters were grouped into 8 clusters based on the matrix of correlation coefficient

836 values. TCR repertoire meta-parameter were calculated by averaging the rank of

837 parameters in each cluster. Meta-parameters were used for correlation analysis.

838 **Quantification and statistical analysis**

839 Statistical analyses were performed using GraphPad Prism (ver9.5.1) software

840 (GraphPad Software). Friedman test with Dunn’s multiple comparisons test was

841 performed on the comparison between the responding patterns of clonotypes or

842 temporal comparison of clonotype frequency. Wilcoxon matched-pairs signed rank test

843 was performed on the comparison of 2nd responder clonotypes after the second and the

844 third shot or comparison of the frequency of S_{448} and S_{1208} tetramer$^+$ cells determined by

845 flow cytometry. The Spearman test was performed on the correlation analysis between

846 repertoire meta-parameters and clinical parameters. Mann-Whitney test was performed

847 on the comparison of the total frequency of S_{448}- and S_{1208}-specific clonotypes

848 determined by tetramer TCR-seq in responding participants. Kruskal-Wallis test with

849 Dunn's multiple comparisons was performed on the comparison of the total frequency

850 of S_{448}-, S_{1208}-, S_{269}-, and S_{919}-specific clonotypes determined by TCR motif analysis in

851 responding participants. q-values are estimated from simultaneous testing (Figure 3H

852 and Figure 5, Supplementary Figure S5) using "qvalue" packaged in R[77]. Asterisks to

853 indicate significance corresponding to the following: ***P<0.001; **P<0.005; *P<0.05;

854 n.s. non-significant (P≥0.05).

855 **Data and materials availability**

856 All sequencing data (Bulk TCRseq, and Single-cell RNA/TCR sequencing) have been

857 deposited at GEO and are publicly available as of the date of publication (GEO:

858 GSE210231). All original code has been deposited at Github (https://github.com/hiro-

859 aoki-mriid/Covid_TCRrepertoire). The list of reagents, antibodies, and algorithms used

860 in this study was summarized in Supplementary Tables S3, 4, and 5, respectively.

861

862 **Acknowledgments**

863 This work was supported by the Japan Society for the Promotion of Science (JSPS)

864 under Grant Numbers 17929397, 20281832, and 22H05064, and Japan Agency for

Medical Research and Development (AMED) under Grant Number JP22fk0310509, JP22ama221306, and P21gm6210025. We want to thank Y. Hara for advice in cell sorting, members of IGT. Inc. for expert technical assistance in TCR sequencing, M. Takahashi, D. Komura, and S. Ishikawa for advice in data analysis. We thank Dr. David L. Woodland for excellent English language editing. Fig. 1A, 1E, 2B, 4E, 6A, and 7A were created with BioRender.com.

Author Contributions

HA, MK, TI, and SU performed conceptualization. HA performed data curation, formal analysis, and visualization. HA and SS developed software. HA, SS, AH, CM, and SU designed the methodology. HA, MK, HA, PX, MT, AH, NOS, and SU conducted a research and investigation process. TI, KM, and SU acquired funds. TI and SU administrated the project. SS and KM supervised the project. HA and SU wrote the original draft, and all the authors participated in writing the final manuscript.

Competing Interests statement

H.A. reports stock for ImmunoGeneTeqs, Inc. S.S. reports advisory role for ImmunoGeneTeqs, Inc; stock for ImmunoGeneTeqs, Inc, T.I. reports research funding

from Rohto Pharmaceutical Co., Ltd., and Biometrics Sympathies Inc. K.M. reports consulting or advisory role for Kyowa-Hakko Kirin, ImmunoGeneTeqs, Inc; research funding from Kyowa-Hakko Kirin, and Ono; stock for ImmunoGeneTeqs, Inc, IDAC Theranostics, Inc. S.U. reports advisory role for ImmunoGeneTeqs, Inc; stock for ImmunoGeneTeqs, Inc, IDAC Theranostics, Inc.

References

1. Han, X., Xu, P., and Ye, Q. (2021). Analysis of COVID-19 vaccines: Types, thoughts, and application. J Clin Lab Anal *35*, 1–7.
2. Sahin, U., Muik, A., Vogler, I., Derhovanessian, E., Kranz, L.M., Vormehr, M., Quandt, J., Bidmon, N., Ulges, A., Baum, A., et al. (2021). BNT162b2 vaccine induces neutralizing antibodies and poly-specific T cells in humans. Nature *595*, 572–577.
3. Pegu, A., O'Connell, S.E., Schmidt, S.D., O'Dell, S., Talana, C.A., Lai, L., Albert, J., Anderson, E., Bennett, H., Corbett, K.S., et al. (2021). Durability of mRNA-1273 vaccine-induced antibodies against SARS-CoV-2 variants. Science (1979) *373*, 1372–1377.
4. Mateus, J., Dan, J.M., Zhang, Z., Moderbacher, C.R., Lammers, M., Goodwin, B., Sette, A., Crotty, S., and Weiskopf, D. (2021). Low-dose mRNA-1273 COVID-19 vaccine generates durable memory enhanced by cross-reactive T cells. Science (1979) *374*, 1–18.
5. Moss, P. (2022). The T cell immune response against SARS-CoV-2. Nat Immunol *23*, 186–193.
6. Skelly, D.T., Harding, A.C., Gilbert-Jaramillo, J., Knight, M.L., Longet, S., Brown, A., Adele, S., Adland, E., Brown, H., Chinnakannan, S., et al. (2021). Two doses of SARS-CoV-2 vaccination induce robust immune responses to emerging SARS-CoV-2 variants of concern. Nat Commun *12*, 1–12.
7. Kedzierska, K., and Thomas, P.G. (2022). Count on us: T cells in SARS-CoV-2 infection and vaccination. Cell Rep Med *3*.

8. Naranbhai, V., Nathan, A., Kaseke, C., Berrios, C., Khatri, A., Choi, S., Getz, M.A., Tano-Menka, R., Ofoman, O., Gayton, A., et al. (2022). T cell reactivity to the SARS-CoV-2 Omicron variant is preserved in most but not all individuals. Cell *185*, 1041-1051.e6.
9. Painter, M.M., Mathew, D., Goel, R.R., Apostolidis, S.A., Pattekar, A., Kuthuru, O., Baxter, A.E., Herati, R.S., Oldridge, D.A., Gouma, S., et al. (2021). Rapid induction of antigen-specific CD4+ T cells is associated with coordinated humoral and cellular immunity to SARS-CoV-2 mRNA vaccination. Immunity *54*, 2133-2142.e3.
10. Guerrera, G., Picozza, M., D'Orso, S., Placido, R., Pirronello, M., Verdiani, A., Termine, A., Fabrizio, C., Giannessi, F., Sambucci, M., et al. (2021). BNT162b2 vaccination induces durable SARS-CoV-2–specific T cells with a stem cell memory phenotype. Sci Immunol *6*, 1–18.
11. Reinscheid, M., Luxenburger, H., Karl, V., Graeser, A., Giese, S., Ciminski, K., Reeg, D.B., Oberhardt, V., Roehlen, N., Lang-Meli, J., et al. (2022). COVID-19 mRNA booster vaccine induces transient CD8+ T effector cell responses while conserving the memory pool for subsequent reactivation. Nat Commun *13*.
12. Özbay Kurt, F.G., Lepper, A., Gerhards, C., Roemer, M., Lasser, S., Arkhypov, I., Bitsch, R., Bugert, P., Altevogt, P., Gouttefangeas, C., et al. (2022). Booster dose of mRNA vaccine augments waning T cell and antibody responses against SARS-CoV-2. Front Immunol *13*.
13. Woodland, D.L. (2004). Jump-starting the immune system: Prime-boosting comes of age. Trends Immunol *25*, 98–104.
14. Masopust, D., Ha, S.-J., Vezys, V., and Ahmed, R. (2006). Stimulation History Dictates Memory CD8 T Cell Phenotype: Implications for Prime-Boost Vaccination. The Journal of Immunology *177*, 831–839.
15. Vezys, V., Yates, A., Casey, K.A., Lanier, G., Ahmed, R., Antia, R., and Masopust, D. (2009). Memory CD8 T-cell compartment grows in size with immunological experience. Nature *457*, 196–199.
16. Fraser, K.A., Schenkel, J.M., Jameson, S.C., Vezys, V., and Masopust, D. (2013). Preexisting High Frequencies of Memory CD8+ T Cells Favor Rapid Memory Differentiation and Preservation of Proliferative Potential upon Boosting. Immunity *39*, 171–183.
17. Wirth, T.C., Xue, H.H., Rai, D., Sabel, J.T., Bair, T., Harty, J.T., and Badovinac, V.P. (2010). Repetitive antigen stimulation induces stepwise transcriptome diversification but preserves a core signature of memory CD8+ T cell

948 differentiation. Immunity *33*, 128–140.
949 18. Kurachi, M., Kakimi, K., Ueha, S., and Matsushima, K. (2007). Maintenance of
950 memory CD8+ T cell diversity and proliferative potential by a primary response
951 upon re-challenge. Int Immunol *19*, 105–115.
952 19. Kitabatake, M., Ouji-Sageshima, N., Sonobe, S., Furukawa, R., Konda, M., Hara,
953 A., Aoki, H., Suzuki, Y., Imakita, N., Nakano, A., et al. (2023). Transition of
954 Antibody Titers after SARS-CoV-2 mRNA Vaccination in Japanese Healthcare
955 Workers. Japanese Journal of Infectious Disease *76*, 72–76.
956 20. Rytlewski, J., Deng, S., Xie, T., Davis, C., Robins, H., Yusko, E., and Bienkowska,
957 J. (2019). Model to improve specificity for identification of clinically-relevant
958 expanded T cells in peripheral blood. PLoS One *14*.
959 21. Betts, M.R., Brenchley, J.M., Price, D.A., De Rosa, S.C., Douek, D.C., Roederer,
960 M., and Koup, R.A. (2003). Sensitive and viable identification of antigen-specific
961 CD8+ T cells by a flow cytometric assay for degranulation. J Immunol Methods
962 *281*, 65–78.
963 22. Reiss, S., Baxter, A.E., Cirelli, K.M., Dan, J.M., Morou, A., Daigneault, A.,
964 Brassard, N., Silvestri, G., Routy, J.P., Havenar-Daughton, C., et al. (2017).
965 Comparative analysis of activation induced marker (AIM) assays for sensitive
966 identification of antigen-specific CD4 T cells. PLoS One *12*, 1–22.
967 23. Thieme, C.J., Anft, M., Paniskaki, K., Blazquez-Navarro, A., Doevelaar, A.,
968 Seibert, F.S., Hoelzer, B., Konik, M.J., Berger, M.M., Brenner, T., et al. (2020).
969 Robust T Cell Response Toward Spike, Membrane, and Nucleocapsid SARS-CoV-
970 2 Proteins Is Not Associated with Recovery in Critical COVID-19 Patients. Cell
971 Rep Med *1*, 100092.
972 24. Galletti, G., De Simone, G., Mazza, E.M.C., Puccio, S., Mezzanotte, C., Bi, T.M.,
973 Davydov, A.N., Metsger, M., Scamardella, E., Alvisi, G., et al. (2020). Two subsets
974 of stem-like CD8+ memory T cell progenitors with distinct fate commitments in
975 humans. Nat Immunol *21*, 1552–1562.
976 25. Abraham, R.S., and Aubert, G. (2016). Flow cytometry, a versatile tool for
977 diagnosis and monitoring of primary immunodeficiencies. Clinical and Vaccine
978 Immunology *23*, 254–271.
979 26. Hamann, D., Baars, P.A., Rep, M.H.G., Hooibrink, B., Kerkhof-Garde, S.R., Klein,
980 M.R., and Van Lier, R.A.W. (1997). Phenotypic and functional separation of
981 memory and effector human CD8+ T cells. Journal of Experimental Medicine *186*,
982 1407–1418.
983 27. Roychoudhuri, R., Clever, D., Li, P., Wakabayashi, Y., Quinn, K.M., Klebanoff, C.A.,

984 Ji, Y., Sukumar, M., Eil, R.L., Yu, Z., et al. (2016). BACH2 regulates CD8 + T cell
985 differentiation by controlling access of AP-1 factors to enhancers. Nat Immunol
986 *17*, 851–860.
987 28. Cui, W., Liu, Y., Weinstein, J.S., Craft, J., and Kaech, S.M. (2011). An interleukin-
988 21- interleukin-10-STAT3 pathway is critical for functional maturation of memory
989 CD8 + T cells. Immunity *35*, 792–805.
990 29. Rush-Kittle, J., Gámez-Díaz, L., and Grimbacher, B. (2022). Inborn errors of
991 immunity associated with defects of self-tolerance checkpoints: The CD28 family.
992 Pediatric Allergy and Immunology *33*.
993 30. Hatano, R., Ohnuma, K., Yamamoto, J., Dang, N.H., and Morimoto, C. (2013).
994 CD26-mediated co-stimulation in human CD8+ T cells provokes effector function
995 via pro-inflammatory cytokine production. Immunology *138*, 165–172.
996 31. Klingel, H., Lauen, M., Krüttgen, A., Imöhl, M., and Kleines, M. (2022). Severity
997 of adverse reactions is associated with T-cell response in mRNA-1273 vaccinated
998 health care workers. Clin Exp Vaccine Res *11*, 121–124.
999 32. Motozono, C., Toyoda, M., Tan, T.S., Hamana, H., Goto, Y., Aritsu, Y., Miyashita,
1000 Y., Oshiumi, H., Nakamura, K., Okada, S., et al. (2022). The SARS-CoV-2 Omicron
1001 BA.1 spike G446S mutation potentiates antiviral T-cell recognition. Nat Commun
1002 *13*.
1003 33. Rowntree, L.C., Petersen, J., Juno, J.A., Chaurasia, P., Wragg, K., Koutsakos, M.,
1004 Hensen, L., Wheatley, A.K., Kent, S.J., Rossjohn, J., et al. (2021). SARS-CoV-2-
1005 specific CD8+ T-cell responses and TCR signatures in the context of a prominent
1006 HLA-A*24:02 allomorph. Immunol Cell Biol *99*, 990–1000.
1007 34. Kared, H., Redd, A.D., Bloch, E.M., Bonny, T.S., Sumatoh, H., Kairi, F., Carbajo,
1008 D., Abel, B., Newell, E.W., Bettinotti, M.P., et al. (2021). SARS-CoV-2-specific
1009 CD8+ T cell responses in convalescent COVID-19 individuals. Journal of Clinical
1010 Investigation *131*.
1011 35. Dash, P., Fiore-Gartland, A.J., Hertz, T., Wang, G.C., Sharma, S., Souquette, A.,
1012 Crawford, J.C., Clemens, E.B., Nguyen, T.H.O., Kedzierska, K., et al. (2017).
1013 Quantifiable predictive features define epitope-specific T cell receptor repertoires.
1014 Nature *547*, 89–93.
1015 36. Goncharov, M., Bagaev, D., Shcherbinin, D., Zvyagin, I., Bolotin, D., Thomas, P.G.,
1016 Minervina, A.A., Pogorelyy, M. V., Ladell, K., McLaren, J.E., et al. (2022). VDJdb
1017 in the pandemic era: a compendium of T cell receptors specific for SARS-CoV-2.
1018 Nat Methods *19*, 1017–1019.
1019 37. Nolan, S., Vignali, M., Klinger, M., Dines, J.N., Kaplan, I.M., Svejnoha, E., Craft,

1020 T., Boland, K., Pesesky, M., Gittelman, R.M., et al. (2020). A large-scale database
1021 of T-cell receptor beta (TCRß) sequences and binding associations from natural
1022 and synthetic exposure to SARS-CoV-2. Res Sq.
1023 38. Mayer-Blackwell, K., Schattgen, S., Cohen-Lavi, L., Crawford, J.C., Souquette, A.,
1024 Gaevert, J.A., Hertz, T., Thomas, P.G., Bradley, P.G., and Fiore-Gartland, A. (2021).
1025 Tcr meta-clonotypes for biomarker discovery with tcrdist3 enabled identification
1026 of public, hla-restricted clusters of sars-cov-2 tcrs. Elife *10*, 1–32.
1027 39. Kaech, S.M., Wherry, E.J., and Ahmed, R. (2002). Effector and memory T-cell
1028 differentiation: Implications for vaccine development. Nat Rev Immunol *2*, 251–
1029 262.
1030 40. Sette, A., and Crotty, S. (2020). Pre-existing immunity to SARS-CoV-2: the knowns
1031 and unknowns. Nat Rev Immunol *20*, 457–458.
1032 41. Grifoni, A., Weiskopf, D., Ramirez, S.I., Mateus, J., Dan, J.M., Moderbacher, C.R.,
1033 Rawlings, S.A., Sutherland, A., Premkumar, L., Jadi, R.S., et al. (2020). Targets
1034 of T Cell Responses to SARS-CoV-2 Coronavirus in Humans with COVID-19
1035 Disease and Unexposed Individuals. Cell *181*, 1489-1501.e15.
1036 42. Weiskopf, D., Schmitz, K.S., Raadsen, M.P., Grifoni, A., Okba, N.M.A., Endeman,
1037 H., van den Akker, J.P.C., Molenkamp, R., Koopmans, M.P.G., van Gorp, E.C.M.,
1038 et al. (2020). Phenotype and kinetics of SARS-CoV-2-specific T cells in COVID-19
1039 patients with acute respiratory distress syndrome. Sci Immunol *5*, 1–11.
1040 43. Bacher, P., Rosati, E., Esser, D., Martini, G.R., Saggau, C., Schiminsky, E.,
1041 Dargvainiene, J., Schröder, I., Wieters, I., Khodamoradi, Y., et al. (2020). Low-
1042 Avidity CD4+ T Cell Responses to SARS-CoV-2 in Unexposed Individuals and
1043 Humans with Severe COVID-19. Immunity *53*, 1258-1271.e5.
1044 44. Masopust, D., Ha, S.-J., Vezys, V., and Ahmed, R. (2006). Stimulation History
1045 Dictates Memory CD8 T Cell Phenotype: Implications for Prime-Boost Vaccination.
1046 The Journal of Immunology *177*, 831–839.
1047 45. Wirth, T.C., Xue, H.H., Rai, D., Sabel, J.T., Bair, T., Harty, J.T., and Badovinac,
1048 V.P. (2010). Repetitive antigen stimulation induces stepwise transcriptome
1049 diversification but preserves a core signature of memory CD8+ T cell
1050 differentiation. Immunity *33*, 128–140.
1051 46. Kay Chung, H., McDonald, B., and Kaech, S.M. (2021). The architectural design
1052 of CD8+ T cell responses in acute and chronic infection: Parallel structures with
1053 divergent fates. Journal of Experimental Medicine *218*.
1054 47. Saggau, C., Martini, G.R., Rosati, E., Meise, S., Messner, B., Kamps, A.K., Bekel,
1055 N., Gigla, J., Rose, R., Voß, M., et al. (2022). The pre-exposure SARS-CoV-2-

1056 specific T cell repertoire determines the quality of the immune response to
1057 vaccination. Immunity *55*, 1924-1939.e5.
1058 48. Brewer, R.C., Ramadoss, N.S., Lahey, L.J., Jahanbani, S., Robinson, W.H., and
1059 Lanz, T. V. (2022). BNT162b2 vaccine induces divergent B cell responses to SARS-
1060 CoV-2 S1 and S2. Nat Immunol *23*, 33–39.
1061 49. Lustig, Y., Gonen, T., Meltzer, L., Gilboa, M., Indenbaum, V., Cohen, C., Amit, S.,
1062 Jaber, H., Doolman, R., Asraf, K., et al. (2022). Superior immunogenicity and
1063 effectiveness of the third compared to the second BNT162b2 vaccine dose. Nat
1064 Immunol *23*, 940–946.
1065 50. Munro, A.P.S., Feng, S., Janani, L., Cornelius, V., Aley, P.K., Babbage, G., Baxter,
1066 D., Bula, M., Cathie, K., Chatterjee, K., et al. (2022). Safety, immunogenicity, and
1067 reactogenicity of BNT162b2 and mRNA-1273 COVID-19 vaccines given as fourth-
1068 dose boosters following two doses of ChAdOx1 nCoV-19 or BNT162b2 and a third
1069 dose of BNT162b2 (COV-BOOST): a multicentre, blinded, phase 2, randomised t.
1070 Lancet Infect Dis *2*, 1131–1141.
1071 51. Andrews, N., Stowe, J., Kirsebom, F., Toffa, S., Rickeard, T., Gallagher, E., Gower,
1072 C., Kall, M., Groves, N., O'Connell, A.-M., et al. (2022). Covid-19 Vaccine
1073 Effectiveness against the Omicron (B.1.1.529) Variant. New England Journal of
1074 Medicine *386*, 1532–1546.
1075 52. Bar-On, Y.M., Goldberg, Y., Mandel, M., Bodenheimer, O., Amir, O., Freedman, L.,
1076 Alroy-Preis, S., Ash, N., Huppert, A., and Milo, R. (2022). Protection by a Fourth
1077 Dose of BNT162b2 against Omicron in Israel. New England Journal of Medicine
1078 *386*, 1712–1720.
1079 53. Oberhardt, V., Luxenburger, H., Kemming, J., Schulien, I., Ciminski, K., Giese, S.,
1080 Csernalabics, B., Lang-Meli, J., Janowska, I., Staniek, J., et al. (2021). Rapid and
1081 stable mobilization of CD8+ T cells by SARS-CoV-2 mRNA vaccine. Nature *597*,
1082 268–273.
1083 54. Pan, Y.G., Aiamkitsumrit, B., Bartolo, L., Wang, Y., Lavery, C., Marc, A., Holec, P.
1084 V., Rappazzo, C.G., Eilola, T., Gimotty, P.A., et al. (2021). Vaccination reshapes the
1085 virus-specific T cell repertoire in unexposed adults. Immunity *54*, 1245-1256.e5.
1086 55. Minervina, A.A., Pogorelyy, M. V., Komech, E.A., Karnaukhov, V.K., Bacher, P.,
1087 Rosati, E., Franke, A., Chudakov, D.M., Mamedov, I.Z., Lebedev, Y.B., et al. (2020).
1088 Primary and secondary anti-viral response captured by the dynamics and
1089 phenotype of individual T cell clones. Elife *9*, 1–21.
1090 56. Nienen, M., Stervbo, U., Mölder, F., Kaliszczyk, S., Kuchenbecker, L., Gayova, L.,
1091 Schweiger, B., Jürchott, K., Hecht, J., Neumann, A.U., et al. (2019). The role of

1092 pre-existing cross-reactive central memory CD4 T-cells in vaccination with
1093 previously unseen influenza strains. Front Immunol *10*.
1094 57. Poon, M.M.L., Rybkina, K., Kato, Y., Kubota, M., Matsumoto, R., Bloom, N.I.,
1095 Zhang, Z., Hastie, K.M., Grifoni, A., Weiskopf, D., et al. (2021). SARS-CoV-2
1096 infection generates tissue-localized immunological memory in humans. Sci
1097 Immunol *6*.
1098 58. Henry, C., Palm, A.K.E., Krammer, F., and Wilson, P.C. (2018). From Original
1099 Antigenic Sin to the Universal Influenza Virus Vaccine. Trends Immunol *39*, 70–
1100 79.
1101 59. Biswas, A., Chakrabarti, A.K., and Dutta, S. (2020). Current challenges: from the
1102 path of "original antigenic sin" towards the development of universal flu vaccines:
1103 Flu vaccine efficacy encounters significant hurdles from pre-existing immunity of
1104 the host suggesting assessment of host immunity before vacci. Int Rev Immunol
1105 *39*, 21–36.
1106 60. Aoki, H., Tsunoda, M., Ogiwara, H., Shimizu, H., Abe, H., Ogawa, T., Abe, T.,
1107 Shichino, S., Matsushima, K., and Ueha, S. (2023). Clonal Spreading of Tumor-
1108 Infiltrating T Cells Underlies the Robust Antitumor Immune Responses. Cancer
1109 Immunol Res, OF1–OF16.
1110 61. Martin, M. (2011). Cutadapt Removes Adapter Sequences From High-Throughput
1111 Sequencing Reads. EMBnet J *17*, 10–12.
1112 62. Schmieder, R., and Edwards, R. (2011). Quality control and preprocessing of
1113 metagenomic datasets. Bioinformatics *27*, 863–864.
1114 63. Bolotin, D.A., Poslavsky, S., Mitrophanov, I., Shugay, M., Mamedov, I.Z.,
1115 Putintseva, E. V., and Chudakov, D.M. (2015). MiXCR: Software for
1116 comprehensive adaptive immunity profiling. Nat Methods *12*, 380–381.
1117 64. Aoki, H., Ueha, S., Shichino, S., Ogiwara, H., Shitara, K., Shimomura, M., Suzuki,
1118 T., Nakatsura, T., Yamashita, M., Kitano, S., et al. (2021). Transient depletion of
1119 CD4þ cells induces remodeling of the TCR repertoire in gastrointestinal cancer.
1120 Cancer Immunol Res *9*, 624–636.
1121 65. Shugay, M., Bagaev, D. V., Turchaninova, M.A., Bolotin, D.A., Britanova, O. V.,
1122 Putintseva, E. V., Pogorelyy, M. V., Nazarov, V.I., Zvyagin, I. V., Kirgizova, V.I., et
1123 al. (2015). VDJtools: Unifying Post-analysis of T Cell Receptor Repertoires. PLoS
1124 Comput Biol *11*, 1–16.
1125 66. Chiffelle, J., Genolet, R., Perez, M.A., Coukos, G., Zoete, V., and Harari, A. (2020).
1126 T-cell repertoire analysis and metrics of diversity and clonality. Curr Opin
1127 Biotechnol *65*, 284–295.

67. Shichino, S., Ueha, S., Hashimoto, S., Ogawa, T., Aoki, H., Wu, B., Chen, C.-Y., Kitabatake, M., Ouji-Sageshima, N., Hontsu, S., et al. (2022). TAS-Seq is a robust and sensitive amplification method for bead-based scRNA-seq. Commun Biol, 5(1), 602.
68. Shen, W., Le, S., Li, Y., and Hu, F. (2016). SeqKit: A cross-platform and ultrafast toolkit for FASTA/Q file manipulation. PLoS One *11*, 1–10.
69. Langmead, B., and Salzberg, S.L. (2012). Fast gapped-read alignment with Bowtie 2. Nat Methods *9*, 357–359.
70. Lun, A.T.L., Riesenfeld, S., Andrews, T., Dao, T.P., Gomes, T., and Marioni, J.C. (2019). EmptyDrops: Distinguishing cells from empty droplets in droplet-based single-cell RNA sequencing data. Genome Biol *20*, 63.
71. Hao, Y., Hao, S., Andersen-Nissen, E., Mauck, W.M., Zheng, S., Butler, A., Lee, M.J., Wilk, A.J., Darby, C., Zager, M., et al. (2021). Integrated analysis of multimodal single-cell data. Cell *184*, 3573-3587.e29.
72. Stuart, T., Butler, A., Hoffman, P., Hafemeister, C., Papalexi, E., Mauck, W.M., Hao, Y., Stoeckius, M., Smibert, P., and Satija, R. (2019). Comprehensive Integration of Single-Cell Data. Cell *177*, 1888-1902.e21.
73. Zheng, Y., Jun, S.-H., Tian, Y., Florian, M., and Gottardo, R. (2022). Robust Normalization and Integration of Single-cell Protein Expression across CITE-seq Datasets. bioRxiv. 10.1101/2022.04.29.489989.
74. Hao, Y., Hao, S., Andersen-Nissen, E., Mauck, W.M., Zheng, S., Butler, A., Lee, M.J., Wilk, A.J., Darby, C., Zager, M., et al. (2021). Integrated analysis of multimodal single-cell data. Cell *184*, 3573-3587.e29.
75. Miller, B.C., Sen, D.R., Al Abosy, R., Bi, K., Virkud, Y. V., LaFleur, M.W., Yates, K.B., Lako, A., Felt, K., Naik, G.S., et al. (2019). Subsets of exhausted CD8+ T cells differentially mediate tumor control and respond to checkpoint blockade. Nat Immunol *20*, 326–336.
76. Song, L., Florea, L., and Langmead, B. (2014). Lighter: fast and memory-efficient sequencing error correction without counting. Genome Biol *15*, 509.
77. Storey, J.D., Bass, A.J., Dabney, A., Robinson, D., and Warnes, G. (2023). qvalue: Q-value estimation for false discovery rate control.

1161 **Figures**

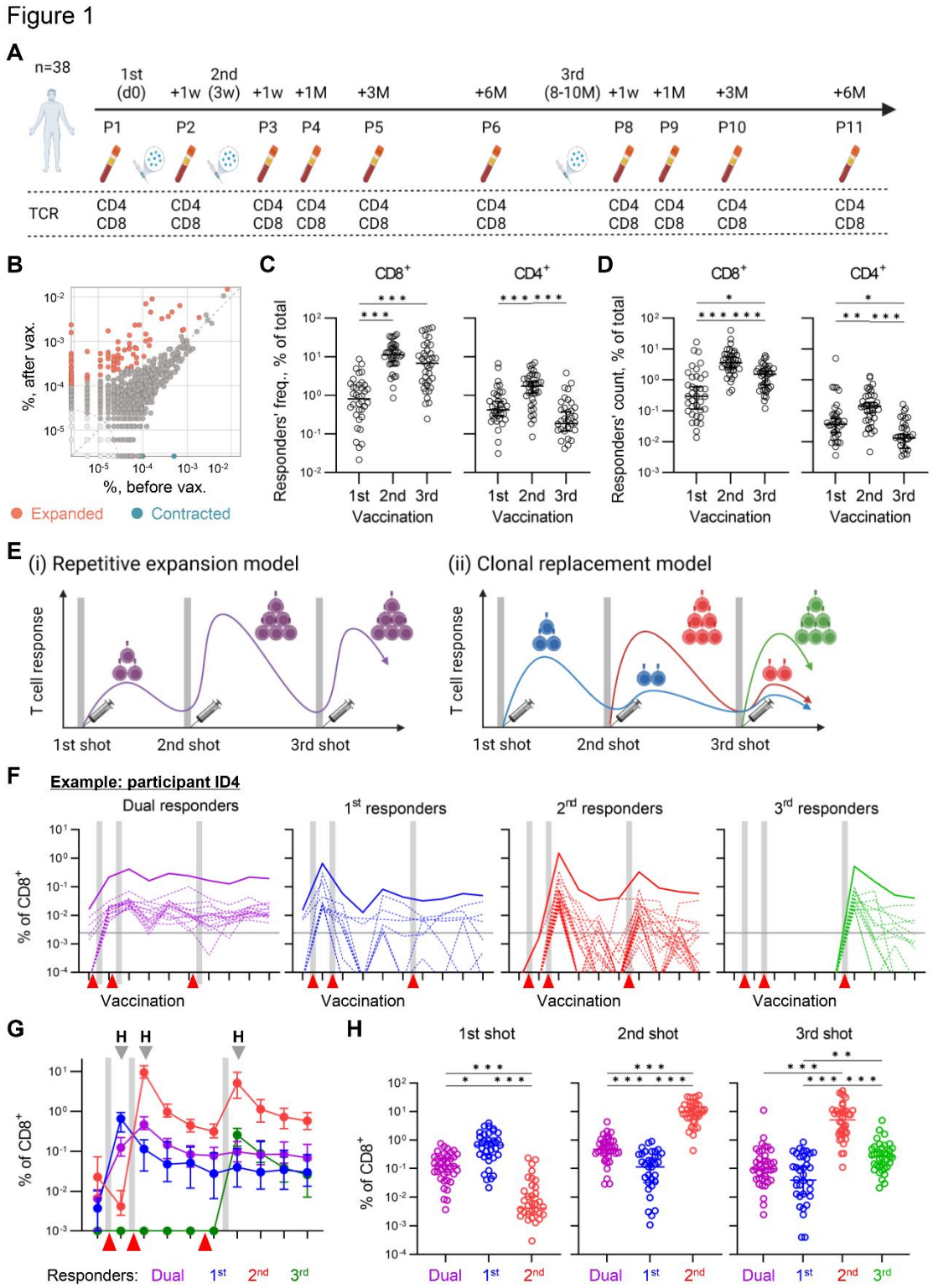

1162

1163 **Fig. 1 Identifying responding clonotypes after vaccination.** (A) Schematic of

1164 longitudinal sample collection before and after BNT162b2 vaccination. Time points for
1165 Bulk TCR-seq (TCR). (B) Example for identifying responding clonotypes using the
1166 beta-binomial model[20]. The scatter plot represents clonotype frequencies in samples
1167 collected before and after vaccination. Significantly expanded (responding) and
1168 contracted clonotypes were indicated as orange and cyan. (C) The total frequency of
1169 $CD8^+$ (left) and $CD4^+$ (right) responding clonotypes after each vaccination. (D)
1170 Diversity of $CD8^+$ (left) and $CD4^+$ (right) responding clonotypes after each vaccination.
1171 The count of responding clonotypes normalized by the total number of clones for each
1172 participant was plotted. (E) Models for T-cell responses following mRNA vaccinations.
1173 (left) Repetitive expansion model: the clonotypes responded to the first shot and
1174 expanded repeatedly after the second and third shots. (right) Clonal replacement model:
1175 primary responder clonotypes were turned over after each vaccination shot. (F)
1176 Classifying $CD8^+$ T-cell clonotypes into 1st, 2nd, dual, and 3rd responders. The frequency
1177 of each clonotype was plotted longitudinally for each type of reaction (dashed lines).
1178 The longitudinal changes of their total frequency were also plotted (thick line). The red
1179 arrows represent the timing of vaccination. The grey horizontal line represents the
1180 threshold for a clonotype to be regarded as "Increased." The data from one participant
1181 (ID4) is shown. (G) Kinetics of $CD8^+$ 1st, 2nd, dual, and 3rd responder clone frequencies.

1182 The median with 95% CI was plotted. (H) The comparison of the total frequency of

1183 $CD8^+$ 1st, 2nd, dual, and 3rd responder clonotypes after each shot. The total frequency for

1184 3rd responders was plotted only after the third shot (right). (C, D, H) Median was

1185 plotted. Friedman test with Dunn's multiple comparison. n = 38 except for P11 (n=37).

1186 ***P<0.001; **P<0.01; *P<0.05. (A) and (E) were created using BioRender.com.

Figure 2

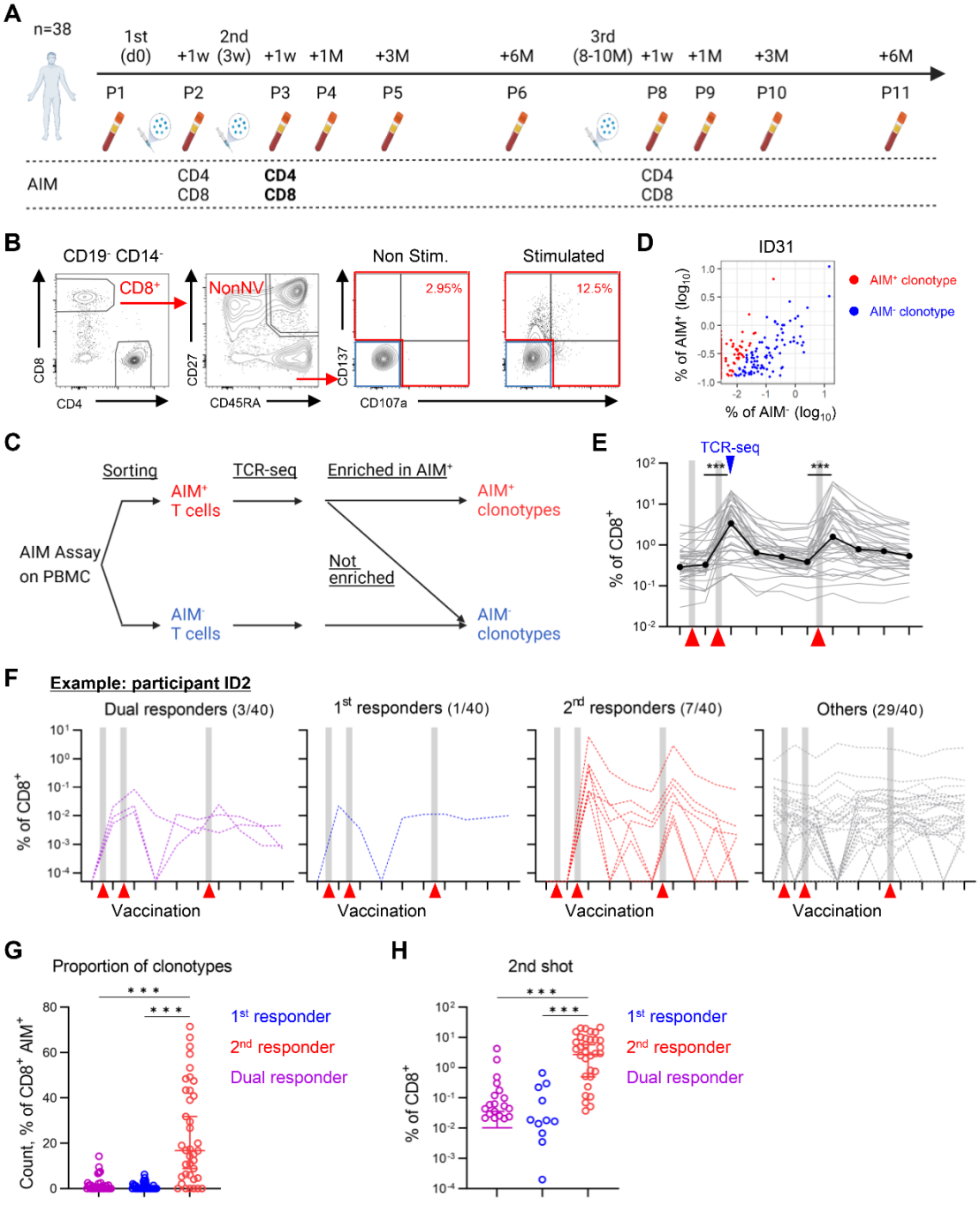

Fig. 2 Response pattern of CD8$^+$ Spike-reactive clonotypes. (A) Schematic of time points of AIM-assay. AIM TCR-seq was performed only on P3 (bold). (B) Gating strategy for sorting AIM$^+$ and AIM$^-$ non-naive CD8$^+$ T cells. The proportion of AIM$^+$

1191 cells among non-naive $CD8^+$ T cells was also shown. (C) Flow chart for identifying

1192 AIM^+ clonotypes. AIM^+ and AIM^- T cells were sorted using the gating as (B), then

1193 TCR-seq was performed on these T cell subsets. AIM^+ clonotypes were identified as

1194 clonotypes that were enriched in the AIM^+ T-cell repertoire (Materials and Methods).

1195 (D) Scatter plot of overlapping clones between AIM^+ and AIM^- repertoire. Individual

1196 dots represent clonotypes with their frequency in AIM^+ and AIM^- repertoire. Red dots

1197 represent AIM^+ clonotypes. (E) Kinetics of the total frequency of $CD8^+$ AIM^+

1198 clonotypes of each participant (thin line, grey). The median was also plotted (thick line,

1199 black). (F) Longitudinal tracking of individual $CD8^+$ AIM^+ clonotypes in one participant

1200 (ID2). Clonotypes were plotted by response patterns (1st responders: blue, 2nd

1201 responders: red, dual responders: purple, and other clonotypes: gray). Numbers indicate

1202 the count of the AIM^+ responder clonotypes and that of all AIM^+ ones. (G) The

1203 proportion of 1st, 2nd, and dual responders in $CD8^+$ AIM^+ clonotypes. The count of AIM^+

1204 responder clonotypes divided by that of all AIM^+ clonotypes was compared. (H) The

1205 total frequency of $CD8^+$ AIM^+ 1st, 2nd, and dual responders after the second vaccination.

1206 (E, G, and H) Friedman test with Dunn's multiple comparisons. n = 38 except for P11

1207 (n=37). ***P<0.001; **P<0.01. (A and C) were created using BioRender.com.

Figure 3

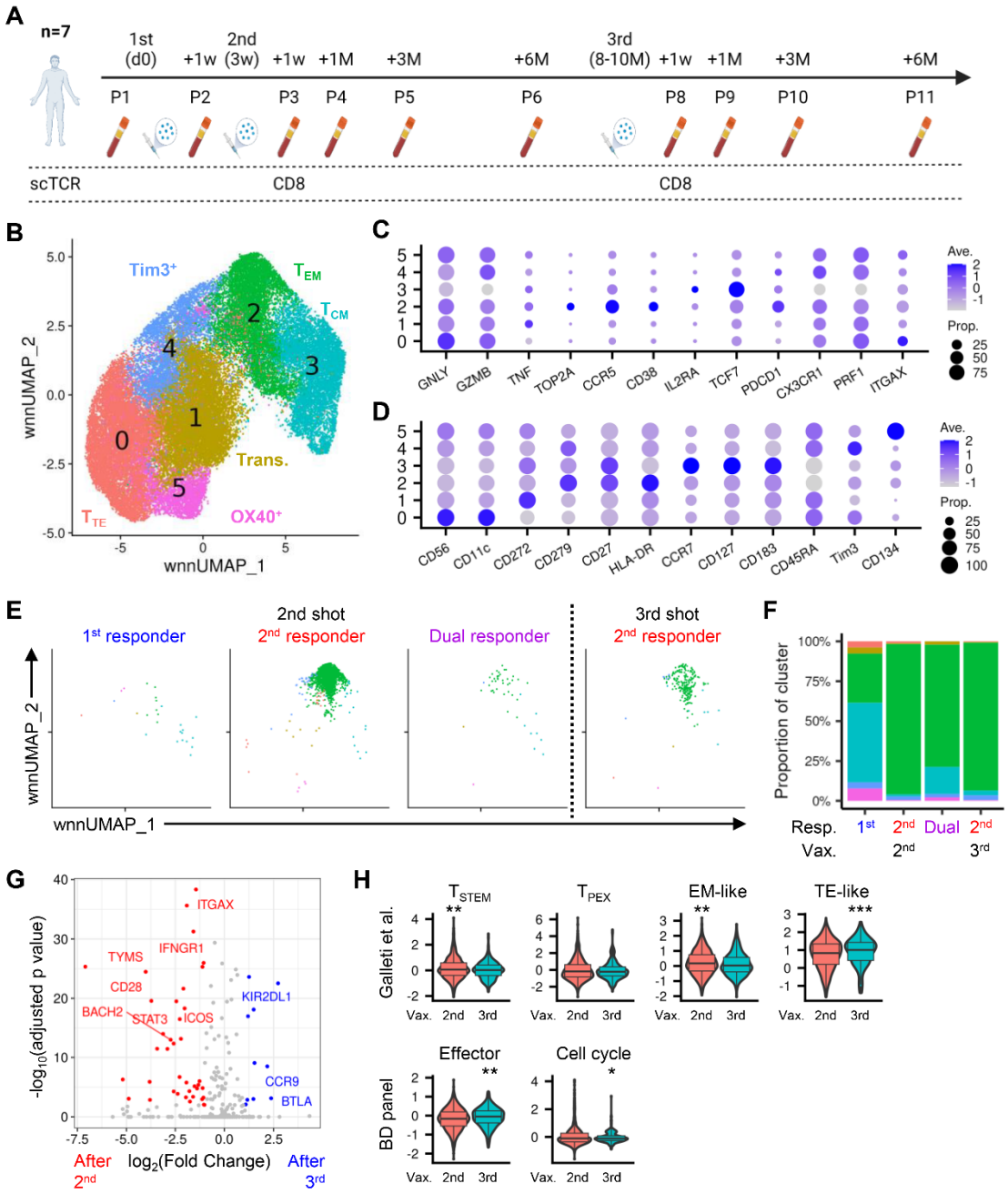

1208

1209 **Fig. 3 Single-cell analysis on non-naive CD8$^+$ T cells after vaccination.** (A)

1210 Schematic of time points of single-cell analysis. (B) Weighted-nearest neighbor graph-

1211 based uniform manifold approximation and projection (wnnUMAP) plot of the

1212 scRNAseq/AbSeq data of non-naive CD8$^+$ T cells. (C and D) Dot plot showing mRNA

1213 (C) and protein (D) expression of marker genes in the T-cell clusters. The size of the

1214 circle shows the percentage of cells in a cluster expressing the gene: color scale shows

1215 the gene expression level. (E) wnnUMAP plot for T cells in 1st, 2nd, and dual responder

1216 clones at TP3 or TP8. (F) Bar graph representing the cluster distribution of T cells in 1st,

1217 2nd, and dual responder clonotypes. (G) Volcano plots of differential expression test of T

1218 cells from TP3 versus TP8 2nd responder clonotypes. Genes expressed more than two-

1219 fold with statistical significance ($p < 0.01$) after the second or third shot are plotted in

1220 red or blue, respectively. (H) Violin plot showing gene signature scores of T cells in 2nd

1221 responder clonotypes at TP3 or TP8. Signature genes are referred from the marker genes

1222 of T-cell clusters described in Galleti et al.[24] and the datasheet of BD Rhapsody™

1223 Immune Response Panel Hs. (H) Student's t-test was performed, and their q-values

1224 were estimated. T_{TE}: terminal effector T cell; Trans: transitional; T_{EM}: effector memory

1225 T cell; T_{CM}: central memory T cell; T_{STEM}: stem-like T cell; T_{PEX}: progenitor exhausted-

1226 like T cell. ***q<0.001; **q<0.01; *q<0.05. (A) was created using BioRender.com.

1227

Figure 4

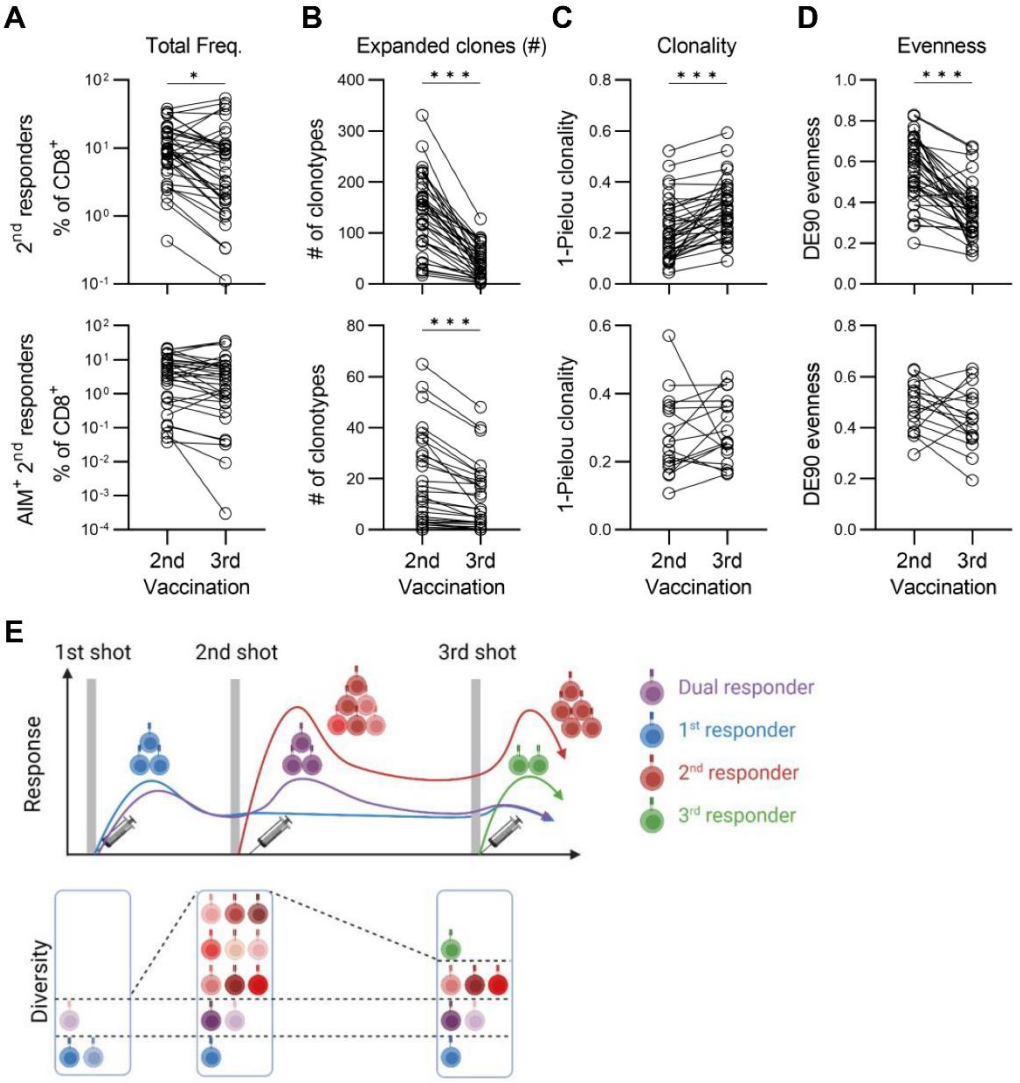

Fig. 4 Re-expansion of CD8$^+$ 2nd responder clonotypes after the third shot. (A) The total frequency of all (top) or AIM$^+$ (bottom) 2nd responders after the second or the third shot. (B) Count of clonotypes that expanded after the second or the third shot within all (top) or AIM$^+$ (bottom) 2nd responders. (C) Clonality of all (top) or AIM$^+$ (bottom) 2nd responders after the second or the third shot. (D) Evenness of all (top) or AIM$^+$ (bottom) 2nd responders after the second or the third shot. (E) Schematic overview for the

1235 response of $CD8^+$ T-cell clonotypes following mRNA vaccination. After the second

1236 shot, 2nd responders turned over 1st responders and became dominant in vaccine-

1237 responding T cells. After the third shot, 2nd responders expanded again, while their

1238 diversity was reduced. 3rd responders also appeared after the third shot and partially

1239 replenished the vaccine-induced T-cell responses. (A-D) Wilcoxon matched-pairs signed

1240 rank test. (C and D) Clonality and evenness are calculated only when more than ten

1241 clonotypes exist. n = 38 except for the bottom of (C) and (D) (n=17). ***P<0.001;

1242 *P<0.05. (E) was created using BioRender.com.

1243

Figure 5

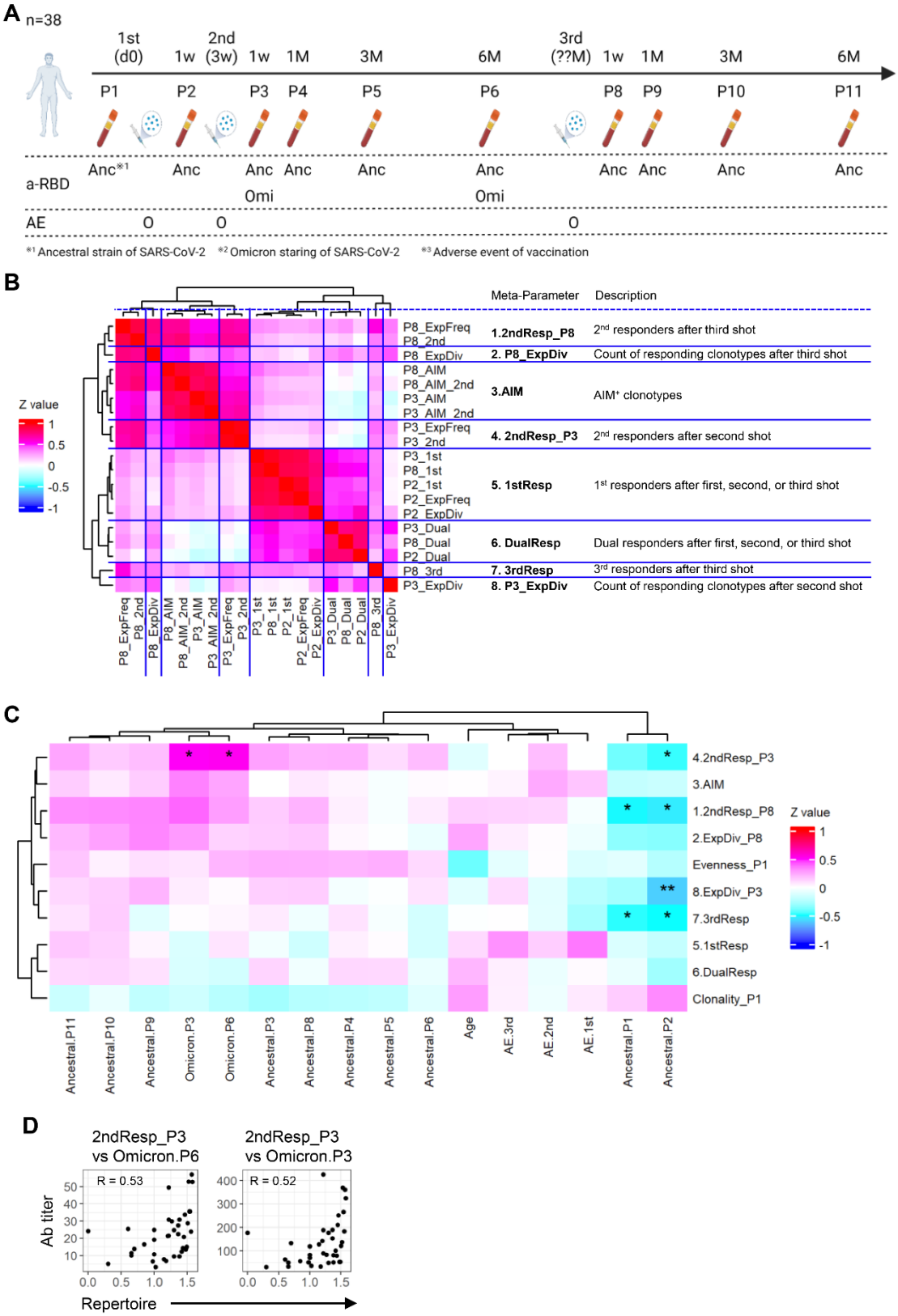

1244

1245 **Fig. 5 Correlation between CD8$^+$ T cell repertoire meta-parameters and other**

1246 **variables regarding vaccination.** (A) Schematic of time points of quantifying serum

1247 anti-RBD antibody titer and checking the presence of adverse vaccination events.

1248 Antibody titers against RBD of SARS-CoV-2 ancestral strain ("Anc") and Omicron

1249 variant ("Omi") were analyzed. (B) Heatmap of the correlation between CD8$^+$ T cell

1250 repertoire parameters. The repertoire meta-parameter is calculated as the average of

1251 mutually correlated repertoire parameters (Materials and Methods). The names of

1252 repertoire meta-parameters and their descriptions are also shown. (C) Heatmap of the

1253 correlation between CD8$^+$ T cell repertoire meta-parameters (row) and the age of

1254 participants, the titer of anti-SARS-CoV-2 RBD IgG antibodies ("Ancestral" or

1255 "Omicron"), or strength of the adverse events ("AE") (column). (D) Correlation

1256 between the repertoire parameters (x-axis) and the IgG antibody titers to RBD of

1257 Omicron variant ("Omicron") of SARS-CoV-2. The Spearman correlation coefficient

1258 between the two parameters is shown. (B and C). The Spearman correlation coefficient

1259 is colored in the heatmap. (C) q-values of the Spearman correlation coefficient between

1260 two parameters are plotted. **$q<0.01$; *$q<0.05$. (A) was created using BioRender.com.

1261

Figure 6

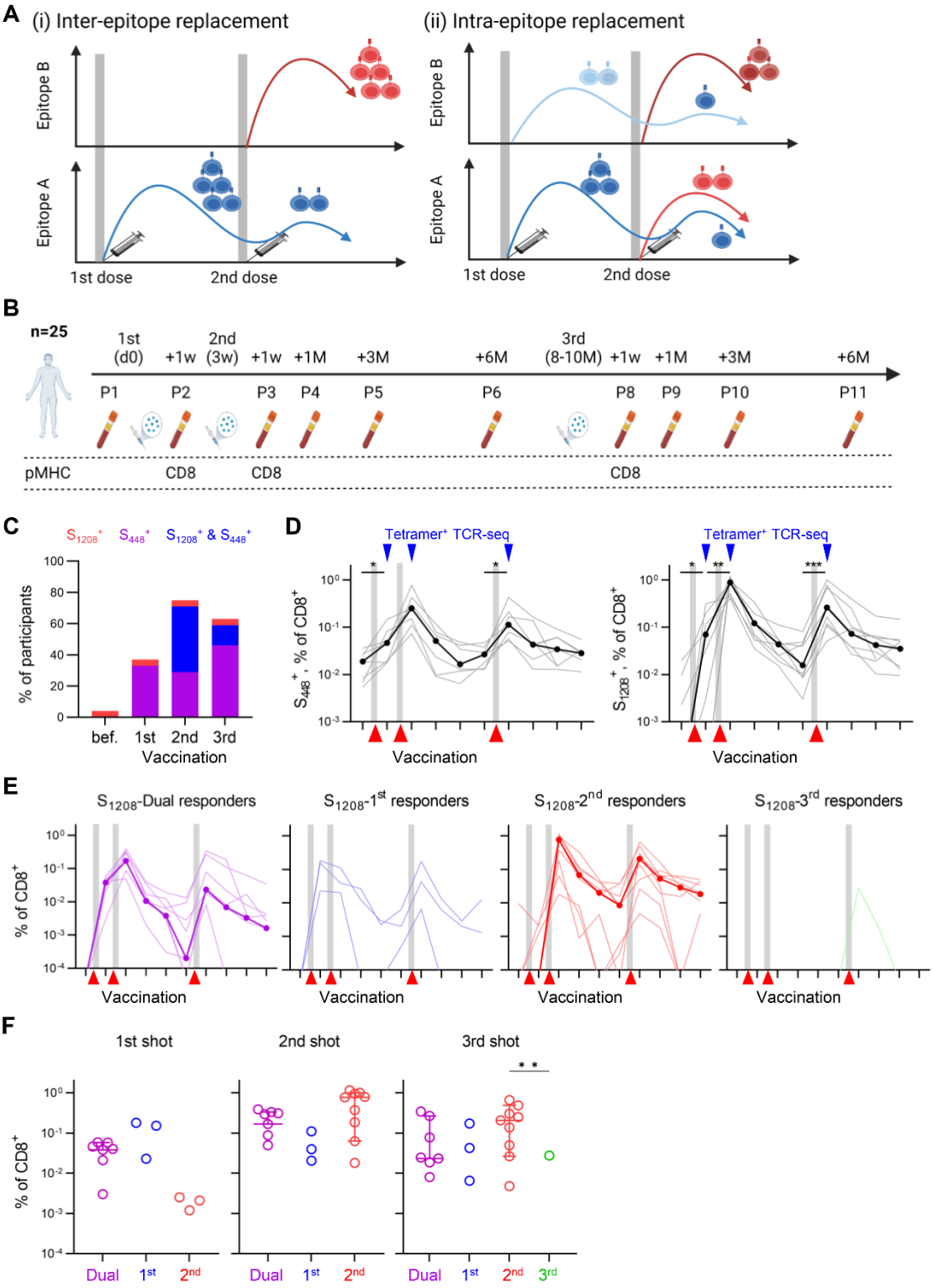

Fig. 6 Analysis of Spike-specific clonotypes using pMHC-tetramer staining. (A) The

1264 working hypothesis for the clonal replacement during mRNA vaccination. (left)

1265 different epitopes induce the 1st and 2nd responder clonotypes (inter-epitope

1266 replacement). (right) Responding clonotypes are changed within each Spike epitope

1267 (intra-epitope replacement). (B) Schematic of time points of Spike peptide-MHC

1268 tetramer analysis. (C) Percentage of participants in whom S_{448} or S_{1208}-specific T-cell

1269 responses were detected by flow cytometry. Spike-specific T-cell responses were

1270 defined as more than 0.1% tetramer$^+$ cells among CD8$^+$ T cells. (D) The total frequency

1271 of CD8$^+$ S_{448}^+ (left) or S_{1208}^+ (right) clonotypes of participants in whom epitope-specific

1272 T-cell responses ("epitope-responsive participants") were detected by repertoire analysis

1273 (thin line, grey). The median was also plotted (thick line, black). Epitope-responsive

1274 participants were defined in Supplementary Figure 6D. (E) Kinetics of S_{1208}-specific 1st,

1275 2nd, dual, and 3rd responder clonotype frequencies. The thin line represents the total

1276 frequency for each participant. The thick line represents the median for S_{1208}-responsive

1277 participants. (F) Comparison of the total frequency of S_{1208}-specific 1st, 2nd, dual, and 3rd

1278 responder clonotypes after each shot. The total frequency for 3rd responders was plotted

1279 only after the third shot (right). n = 7 and 9 for S_{448}- or S_{1208}- responsive participants,

1280 respectively. (D and F) Friedman test with Dunn's multiple comparisons was performed.

1281 ***P<0.001; **P<0.01; *P<0.05. (A and B) were created using BioRender.com.

Figure 7

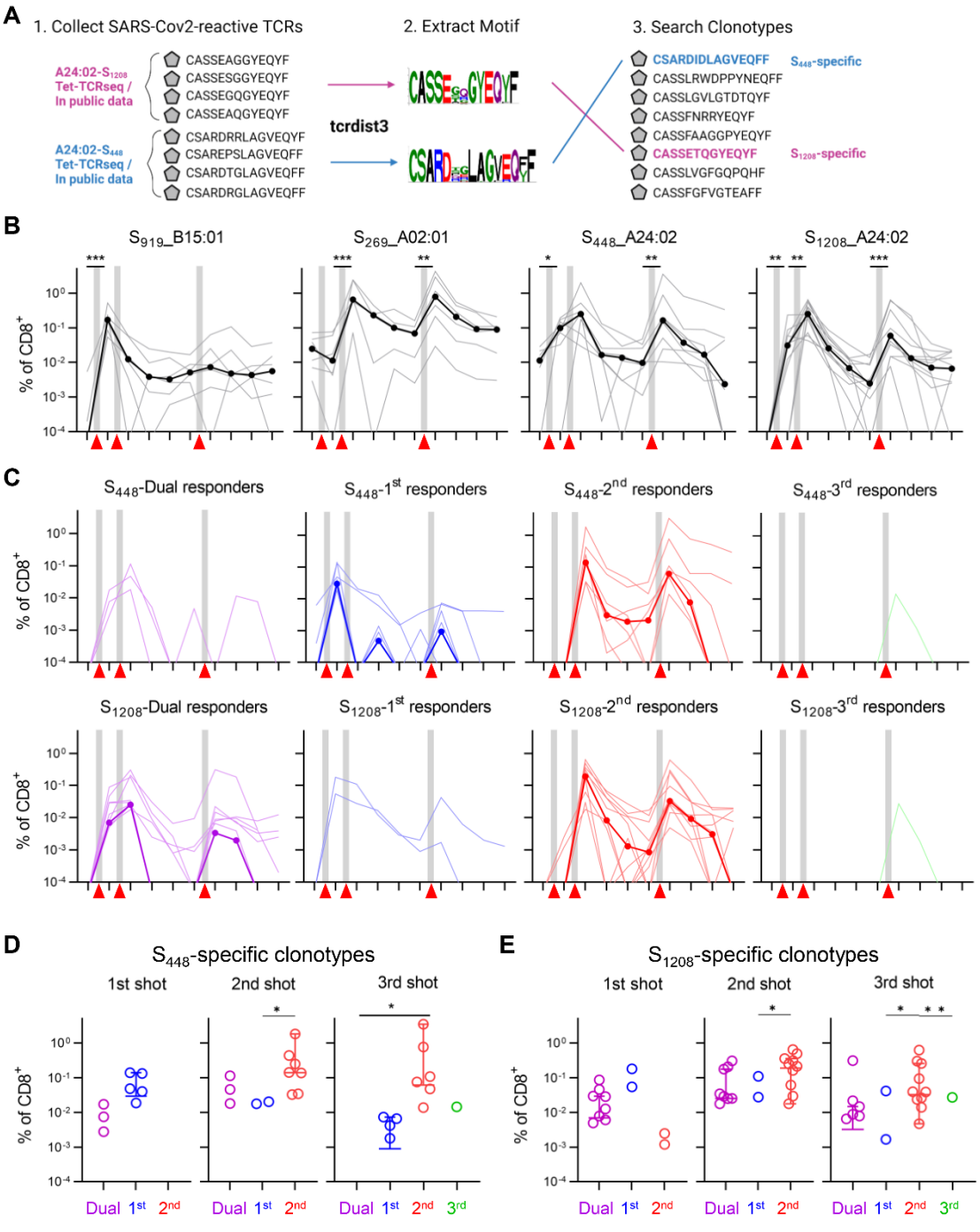

Fig. 7 Analysis of Spike-specific clonotypes using TCR sequence motifs. (A) Schematic overview. (left) We used Spike-specific TCRs in three public databases and our original Tetramer-TCRseq datasets as input. (middle) Shared TCR sequence motifs

1286 of Spike-specific clonotypes were constructed using the tcrdist3 pipeline[38]. TCR

1287 sequence motifs are represented as logo plots, where the sizes and colors of the letters

1288 represent the frequency and characteristics of amino acids (red: acidic, blue: basic,

1289 green: polar, purple: neutral, black: hydrophobic). (right) T cell clonotypes possessing

1290 the Spike-specific TCR sequence motifs were searched. When searching clonotypes

1291 with sequence motif specific to each Spike-epitope, only participants with HLA that

1292 presents the epitope were analyzed. (B) The total frequency of $CD8^+$ S_{448}, S_{1208}, S_{269}, or

1293 S_{919}-specific clonotypes of epitope-responsive participants (thin line, grey). The median

1294 was also plotted (thick line, black). Epitope-responsive participants were defined in

1295 Supplementary Figure 6D. (C) Kinetics of S_{448}- (top) or S_{1208}- (bottom) specific 1st, 2nd,

1296 dual, and 3rd responder clonotype frequencies. The thin line represents the total

1297 frequency for each participant. The thick line represents the median for epitope-

1298 responsive participants. (D and E) Comparison of the total frequency of S_{448}- (D) or

1299 S_{1208}- (E) specific 1st, 2nd, dual, and 3rd responder clonotypes after each vaccination. The

1300 total frequency for 3rd responders was plotted only after the third shot. n = 8 (S_{448}), 12

1301 (S_{1208}), or 6 (S_{269} and S_{919}). (B, D, and E) Friedman test with Dunn's multiple

1302 comparisons. ***P<0.001; **P<0.01; *P<0.05. (A) was created using BioRender.com.

1303